On the Use of CFCs in an Oceanic General Circulation Model

by

Daniel Robitaille

B.Sc., Université de Montréal, Montréal, 1991

M.Sc., McGill University, Montréal, 1993

A Thesis Submitted in Partial Fulfillment of the

Requirements for the Degree of

MASTER OF SCIENCE

in the School of Earth and Ocean Sciences

Supervisor: Dr. Andrew J. Weaver

ABSTRACT

The use of Chlorofluorocarbons (CFCs) in ocean modelling is evaluated for different kinds of models and configurations. These models range from an idealized basin model to a global ocean model. In the later case, the CFC-11 concentrations in the global ocean model are compared to observations when using three different sub-grid-scale mixing parameterizations: a lateral/vertical scheme; an isopycnal scheme; and the Gent and McWilliams scheme. The Gent and McWilliams scheme improves the CFC-11 distributions when compared to both of the other schemes. The main improvement comes from a reduction of CFC uptake in the Southern Ocean.

Table of Contents

List of Tables

List of Figures

1. Introduction

Traditionally the results from oceanic general circulation models are analyzed by examining streamfunctions, heat and salt transports and fluxes, and temperature and salinity fields. For this thesis, the use of passive tracers to help validate and analyze the enormous amount of data an ocean model can generate is examined. The passive tracer used is CFC-11 but the method may be extended to include other passive tracers to facilitate more diverse comparisons between observations and model output.

In section 2 an introduction to CFCs and their history as oceanic tracers is first presented. Following this, the theory behind the method used to introduce CFCs into an ocean method is examined. Next, a look at the atmospheric concentration of CFC-11 since the start of production in the early 1930s, is given. Section 2.3 will look at the solubilities of CFC-11, mainly following the work presented in Warner and Weiss (1985). Section 2.4 will examine two methods to obtain a value for the air-sea gas exchange coefficient from wind speed: the method presented in Liss and Merlivat (1986); and the one contained in the work of Wanninkhof (1992). Finally in section 2.5, a brief look at some of the numerical models using CFCs found in the literature is presented. These models range from simple box models to global ocean models.

Presented in section 3 are some of the results from different kinds of numerical models. The fundamental equations of the models and the three sub-grid-scale mixing schemes used are first examined. Section 3.1 will present some of the results obtained using an idealized basin model. Using this simple model, results from two air-sea gas exchange coefficient methods (section 2.4) will be compared. More complexity is added by using a high resolution (1° x 1°) model of the North Atlantic. This model is employed, using realistic CFC-11 intakes at the surface, to produce a CFC-11 section. The results are examined and compared to observations in section 3.2. In section 3.3, the results from a

global model are given (these results first appeared in Robitaille and Weaver, 1995). Three different sub-grid-scale mixing schemes are utilized: a lateral/vertical mixing scheme; an isopycnal scheme (following the work of Redi, 1982), and a mixing scheme proposed by Gent and McWilliams (1990). A summary and conclusions are found in section 4.

2. Chlorofluorocarbons in ocean modeling

2.1 Introduction

In the 1970s, dissolved atmospheric chlorofluorocarbons (CFC) emerged as very useful time-dependent tracers of processes occurring in the oceans on annual and decadal time scales. The two main CFCs used as tracers are CFC-11 (CCl_3F or trichlorofluoromethane) and CFC-12 (CCl_2F_2 or dichlorodifluoromethane). Their usefulness comes from the fact that CFCs have no known natural sources, and are very stable in the troposphere and in the ocean. CFC-11 and 12 can be destroyed photochemically by ultraviolet light in the stratosphere. This process may be affecting the ozone layer which is the main reason why CFC-11 and CFC-12 in the atmosphere have been closely monitored in the last 20 years or so.

Widespread industrial production of CFCs started in the 1940s (Hart and Conia, 1987) when it was discovered that they were very efficient chemical products to use when spreading insecticides, such as DDT, in the air. The production increased dramatically in the 1970s as their use in various aerosols (paint, deodorant, insecticides, etc.) and in cooling devices became popular. Their presence in manufactured goods has since been reduced, mainly because of a possible link between the reduction of the ozone layer around the earth and the presence of CFCs in the stratosphere.

After their release in the atmosphere, CFCs advect and convect upward, and once in the stratosphere they lose one chlorine atom when photolyzed by solar radiation (Cicerone *et al.*, 1974). Reactions involving chlorine reduce the amount of stratospheric ozone which is a natural ultraviolet screen between the Sun and the Earth's surface.

The use of CFCs as oceanic tracers was first suggested by Lovelock *et al.* (1973). In that study, surface atmospheric and sea-water concentration measurements of CFC-11 were obtained in the Atlantic between 60°N and 70°S. Also, limited measurements below the surface (down to 300 metres), at 14°N and 29°N, showed a decrease in concentration of CFC-11 with an e-folding depth of 130 metres.

One of the first true oceanic profiles of CFC-11 and 12 was obtained by Hahne *et al.* (1978) in the Norwegian Sea. Even though they had contamination problems with their samples, they showed that CFCs could be very useful tracers. For example, by using the CFC-11/CFC-12 concentration ratio for a water mass, and a known atmospheric CFC history, the temperature of the water mass at the time of last contact with the ocean surface can be determined.

The first "modern" studies of CFCs in the oceans (with less contaminated measurements), are the ones by Gammon *et al.* (1982) and Bullister and Weiss (1983). These two studies can be seen as the foundation of nearly all the following studies of CFCs as oceanic tracers. Gammon *et al.* (1982) looked at the vertical distributions of CFC-11 and 12 in the Northeast Pacific ocean in 1980, and were able, by using a simple steady state model, to estimate the vertical diffusivity and upwelling velocities in the thermocline. Bullister and Weiss (1983), using 1982 observations of CFC-11 and 12 in the Greenland and Norwegian Seas, and a time-dependent box model, determined a time-scale for the deep convection in the Greenland Sea of ~40 years, and a time-scale for the lateral mixing between the deep portions of the Greenland and Norwegian Sea of about 20 to 30 years.

2.2 Atmospheric concentration of CFC-11

The atmospheric concentration of CFC-11 has increased continuously since initial production in the 1930s. Atmospheric concentrations of CFC-11 in the Northern Hemisphere are shown in Figure 1. The Southern Hemisphere shows a similar trend, but with a lag of just over one year between the two hemispheres (resulting from the fact that most of the industrial sources of CFCs are located in the Northern Hemisphere). Between 1931 and 1981, the concentration data are based on release figures compiled by the Chemical Manufacturers Association. From these figures, the atmospheric concentrations are found supposing that: 95% of the CFC release occurred in the Northern Hemisphere; that the atmospheric lifetimes for CFC-11 is 74 years (Cunnold *et al.*, 1986); and that the exchange time between the two hemispheres is 1.25 years. From 1981 to the present, the concentrations are based on direct measurements. For the Northern Hemisphere, the measurements are from Mace Head (Ireland) and Cape Meares (Oregon), except after June 1989 when only the Mace Head data is available. For the Southern Hemisphere, the values are from a station at Cape Grim, Tasmania. These atmospheric concentrations are calibrated to the SIO 1986 (Scripps Institute of Oceanography) calibration scale.

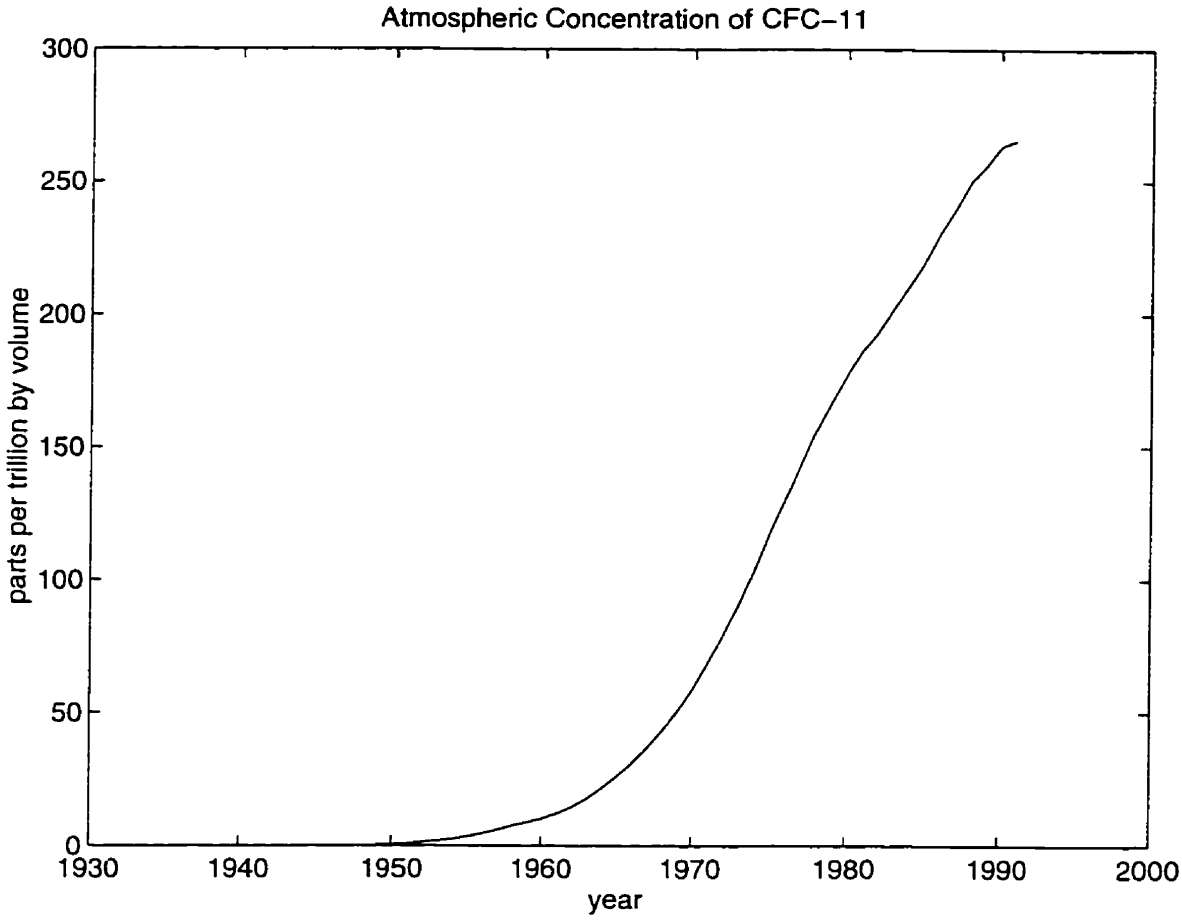

Figure 1. Atmospheric concentration of CFC-11 in the Northern Hemisphere in parts per trillion by volume (R.F. Weiss, personal communication, see Table A-1 for actual figures).

2.3 Solubility of CFC-11

The atmospheric concentrations of CFCs can be linked to their concentrations in the surface waters by using their respective solubilities. Some studies have been done in the past to try to determine the solubility of CFC-11 under different temperatures and salinities. Hunter-Smith *et al.* (1983) measured the solubility of CFC-11 in fresh water and sea water (Salinity S≈35‰) at temperatures between 5°C and 33°C. Wisegarver and Cline (1985) measured the solubility of CFC-11 in seawater (S≈35‰) between 0°C and 32°C, and in fresh water at 25°C. But the study of CFC-11 solubility most often referred to is that of Warner and Weiss (1985), in which the authors present the solubility of CFC-11 for fresh water and sea water (salinity between 0‰ and 40‰) for water temperatures between -1°C and 40°C. The following discussion will parallel the results from the aforementioned.

The concentration of dissolved CFC for the equilibrated surface water in volumetric (mol l^{-1}) or gravimetric (mol kg^{-1}) units, C_{esw} is given by

$$C_{esw} = K'x'\left(P - p_{H_2O}\right) \qquad (1)$$

where K' is a function obtained from surface water temperature and salinity (equation 2), x' is the dry air mole fraction of the CFCs in the atmosphere, P is the total pressure in atmosphere (atm), and p_{H2O} is the water vapour pressure in atm. Equation 1 is valid only for x'« 1 and total pressures near 1 atm. An equation was fitted to observed K' values and has the form

$$\ln K' = a_1 + a_2(100/T) + a_3\ln(T/100) + S\left[b_1 + b_2(T/100) + b_3(T/100)^2\right] \qquad (2)$$

where K' can be in mol l^{-1} atm^{-1} or in mol kg^{-1} atm^{-1}, T is the absolute temperature, S is the salinity in parts per thousand. The subscripted a and b coefficients are given in Table 1 for CFC-11.

The solubilities of CFC-11 can also be expressed in terms of the solubility function F, which is defined by the equation

$$C_{esw} = x'F \tag{3}$$

This relation is valid for a substance with x'«1 in moist air at the water-saturated interface. For a total pressure of 1 atm, F can be found using Equation 4 with the coefficients in table 2:

$$\begin{aligned} \ln F = {} & a_1 + a_2(100/T) + a_3\ln(T/100) + a_4(T/100)^2 \\ & + S\left[b_1 + b_2(T/100) + b_3(T/100)^2\right] \end{aligned} \tag{4}$$

The coefficients in Table 1 and 2 were found by a least-squares fitting of the Equations 2 and 4 to experimental results (Warner and Weiss, 1985).

Table 1. Coefficients for use in Equation 2 to calculate K' (in volumetric or gravimetric units) for CFC-11.

	K' (mol l^{-1} atm^{-1})	K' (mol kg^{-1} atm^{-1})
a_1	-134.1536	-136.2685
a_2	203.2156	206.1150
a_3	56.2320	57.2805
b_1	-0.144449	-0.148598
b_2	0.092952	0.095114
b_3	-0.0159977	-0.0163396

Table 2. Coefficients for use in Equation 4 to calculate F (in volumetric or gravimetric units) for CFC-11 in moist air at a total pressure of 1 atm.

	F (mol l^{-1} atm^{-1})	F (mol kg^{-1} atm^{-1})
a_1	-229.9261	-232.0411
a_2	319.6552	322.5546
a_3	119.4471	120.4956
a_4	-1.39165	-1.39165
b_1	-0.142382	-0.146531
b_2	0.091459	0.093621
b_3	-0.0157274	-0.0160693

2.4 Air-Sea Gas Exchange

The calculated concentrations of CFCs in the upper layer of a model are a function of the gas exchange between the equilibrated surface layer and the upper layer of the model. Some studies have been done in an attempt to relate gas exchange to wind speed, two of which will be presented here. In Liss and Merlivat (1986), a relation was proposed between the gas exchange coefficient (k) and the wind speed of the form:

$$\begin{aligned} k &= 0.17\,u && \text{for } u \le 3.6 \\ k &= 2.85\,u - 9.65 && \text{for } 3.6 < u \le 13 \\ k &= 5.9\,u - 49.3 && \text{for } u > 13 \end{aligned} \qquad (5)$$

where k is in cm h^{-1}, and u is in m s^{-1} and taken at a height of 10 m. This relation was based on various field and laboratory results. Equation 5 is good for a gas with a Schmidt number (Sc) of 600 (the value for CO_2 at 20°C in fresh water). It can be generalized to any gas by multiplying the equation by the term $(Sc/600)^{-1/2}$ where Sc is a function of the gas under study.

Wanninkhof (1992) proposed instead the following relation:

$$k = a\,u^2(Sc/660)^{-1/2} \qquad (6)$$

where u and Sc are as before, and a is a constant equal to 0.39, when using long-term averaged wind speeds, and equal to 0.31 when using instantaneous wind speeds. This relation was found by using various bomb- and natural-^{14}C observations.

The Schmidt number is a unitless constant, defined as the kinematic viscosity of water divided by the molecular diffusivity of the gas. Wanninkhof (1992) gives this relation for the Schmidt number:

$$Sc = A - Bt + Ct^2 - Dt^3 \qquad (7)$$

where t is in degrees Celsius, and the four constants are given in Table 3. These constants were derived by fitting a third-order polynomial through various Schmidt number estimates.

Table 3. Coefficients for use in Equation 7 for CFC-11 for freshwater and seawater (S=35‰) for temperatures ranging from zero to 30 °C.

	A	B	C	D
	Seawater			
CFC-11	4039.8	264.70	8.2552	0.10359
	Freshwater			
CFC-11	3723.7	248.37	7.8208	0.098455

Which of the two formulations is the best? According to Butler *et al.* (1991), Equation 5 under-estimates the dissolved $^{14}CO_2$ by a factor 1.8 when the equations are applied to a global scale. This discrepancy does not occur when using Equation 6. Also, some modelling experiments indicate that there is a greater contribution by low winds in reality as opposed to the formulation by Liss and Merlivat (1986). In their paper, Butler *et al.* (1991) conclude that the Wanninkhof equation provides a more accurate representation of the transfer velocity distribution with wind speed. They also indicate than the uncertainty is very large, and could very well be in the ±50% range.

2.5 Numerical models using CFCs in the ocean as found in the literature

In the literature, the majority of the numerical ocean models involving CFCs are box models using the concentrations of CFCs to study a physical process in a relatively small region. Examples of these kinds of models can be found in Schlosser *et al.* (1991), Bullister and Weiss (1983), Smethie *et al.* (1988), and Rhein (1991) (four studies of the deep-water formation in the Greenland/Norwegian Seas),Warner and Weiss (1992) (study of the Antarctic Intermediate Water in the south-eastern Atlantic), and Wallace and Moore (1985) (study of the Canadian Basin of the Arctic Ocean).

In these box models, the CFCs are generally introduced using solubility equations similar to Equation 3 with atmospheric CFC data. The calculated surface concentration of dissolved CFCs is then modified using some observational data. Usually this modifying factor is the observed concentration of CFCs at one point in time, or the saturation percentage observed in the region under study.

In the box model presented in Trumbore *et al.* (1991), in addition to a solubility equation (Equation 3), they used air-sea gas exchange rates (varying with wind speed) as in Equations 5 and 6. This gives an equation for the concentration of CFCs of the form:

$$h\frac{dC}{dt} = k\left(C_{esw} - C\right) \tag{8}$$

where C is the concentration of CFCs in the upper box in contact with the atmosphere, h is the thickness of the upper box, k is the air-sea gas exchange rate, and C_{esw} is the surface concentration of equilibrated water (as given by Equation 3).

Roether *et al.* (1994) presented one of the first published studies of an ocean general circulation model (OGCM) using CFCs as tracer data. The model they used is the GFDL Bryan-Cox model, applied to the Eastern Mediterranean with a resolution of 1/4° in longitude and latitude, and 19 levels in the vertical. The model is forced by prescribing

climatological monthly temperature and salinity fields and wind stress at the upper boundary. CFC-12 is introduced in the model with an upper boundary condition of solubility equilibrium with the time-dependent atmospheric concentration. The model showed no deep-water formation of Adriatic Water. This situation in their model was rectified by either changing the surface boundary conditions, changing the convection scheme, or by modifying the topography.

England *et al.* (1994), England (1995), and Robitaille and Weaver (1995) presented numerical work using CFCs in a world ocean model. England *et al.* (1994) presented the results for runs using CFC-11 and CFC-12 in a numerical model using a lateral/vertical mixing scheme. They looked at the effects of different methods for introducing CFCs into an OGCM. In the first experiment, the CFC concentrations in the first level of the model were set to their saturation values. This tended to over-estimate the ocean uptake of CFCs. In a second experiment, a constant gas exchange coefficient was used, in a similar fashion to the way temperature and salinity were forced at the surface in a model using a restoring boundary condition. They used a restoring time-scale of ~20 days. In a third experiment, the influence of the sea-ice in polar regions was analyzed by decreasing the air-sea gas exchange rate in ice-covered regions. And finally, in a fourth experiment the Wanninkhof (1992) wind-speed dependent gas exchange rate (Equation 6) was used in combination with a sea-ice cover dependence. In Robitaille and Weaver (1995 -- see section 3.3) and England (1995), the CFC uptake in a model using three different mixing schemes and the implications of these results on climate models was examined. Essentially, it was showed that different sub-grid-scale mixing parameterization have the potential to considerably modify the CFC uptake in a climate model. These changes in uptake could have repercussions on the CO_2-induced warming predicted by climate models using similar kinds of sub-grid-scale mixing schemes.

3. Numerical experiments

This section will present some experiments done with different numerical models in which CFC 11 and 12 were introduced. As shown in the previous section, CFC tracers are generally introduced in a numerical model by using the solubility Equation 3, with a varying atmospheric concentration (from Table A-1). The gas exchange rate can be specified (using a restoring time scale, as will be done with temperature and salinity), or by using a varying exchange rate which is a function of the local winds (Equations 5 or 6). The first model configuration is an idealized basin model of the North Atlantic using the Modular Ocean Model (MOM, version 1.1) developed at GFDL (Pacanowski *et al.*, 1993). This model is an updated version of the model discussed in Bryan (1969), Cox (1984), and Semtner (1986). The model solves the primitive equations under the Boussinesq, hydrostatic, and rigid lid approximation. We can then formulate the equations the model solves in spherical coordinates, with ϕ the latitude (positive northward, and zero defined at the equator), λ the longitude (positive eastward, and zero defined at Greenwich), and the depth z (positive upward, and zero defined at the ocean surface):

$$u_t + L(u) - \frac{uv \cdot \tan\phi}{a} - fv = -\frac{1}{\rho_o a \cdot \cos\phi} p_\lambda + \left(\kappa_m u_z\right)_z + F^u \tag{9a}$$

$$v_t + L(v) - \frac{u^2 \cdot \tan\phi}{a} + fv = -\frac{1}{\rho_o a} p_\phi + \left(\kappa_m v_z\right)_z + F^v \tag{9b}$$

$$T_t + L(T) = \left(\kappa_h \cdot T_z\right)_z + \nabla \cdot \left(A_h \nabla T\right) \tag{9c}$$

$$S_t + L(S) = \left(\kappa_h \cdot S_z\right)_z + \nabla \cdot \left(A_h \nabla S\right) \tag{9d}$$

$$w_z = -\frac{1}{a \cdot \cos\phi} \cdot \left(u_\lambda + \left(\cos\phi \cdot v\right)_\phi\right) \tag{9e}$$

$$p_z = -\rho \cdot g \tag{9f}$$

$$\rho = \rho(T,S,p) \tag{9g}$$

where the horizontal friction terms, advection and horizontal diffusion terms are given by

$$F^u = \nabla\cdot(A_m\nabla u) + A_m\left[\frac{(1-\tan^2\phi)\cdot u}{a^2} - \frac{2\sin\phi\cdot v_\lambda}{a^2\cos^2\phi}\right] \tag{10a}$$

$$F^v = \nabla\cdot(A_m\nabla v) + A_m\left[\frac{(1-\tan^2\phi)\cdot v}{a^2} - \frac{2\sin\phi\cdot u_\lambda}{a^2\cos^2\phi}\right] \tag{10b}$$

$$L(\alpha) = \frac{1}{a\cdot\cos\phi}\cdot(u\cdot\alpha)_\lambda + \frac{1}{a\cdot\cos\phi}\cdot(\cos\phi\cdot v\cdot\alpha)_\phi + (w\cdot\alpha)_z \tag{10c}$$

$$\nabla^2\alpha = \frac{1}{a^2\cos^2\phi}\alpha_{\lambda\lambda} + \frac{1}{a^2\cos\phi}(\cos\phi\cdot\alpha_\phi)_\phi \tag{10d}$$

$$f = 2\Omega\sin\phi \tag{10e}$$

T and S are the potential temperature and salinity, (u,v,w) are the zonal, meridional, and vertical velocities, p is the pressure, ρ the potential density, g is gravitational acceleration, a is the mean radius of the earth, Ω is the earth's rotation rate, A_m and A_h are the horizontal eddy viscosity and diffusivity, and κ_m and κ_h are the vertical viscosity and diffusivity.

The GFDL MOM code solves these equations on a horizontal Arakawa B-grid and a vertical Arakawa C-grid using a centred spatial and leap-frog temporal differencing scheme, with the diffusion terms lagged by one time step (forward Euler) for stability purposes. The horizontal diffusion and viscosity terms are solved explicitly, while the vertical diffusion and viscosity are solved implicitly. The Coriolis term is handled semi-implicitly.

To parameterize sub-grid-scale mixing effects, three schemes will be considered. The lateral/vertical mixing scheme (denoted HOR – see Equations 9c and 9d) is often used in z-coordinate ocean models as it is the simplest possible mixing parameterization. Since

mixing in the real ocean is predominantly along isopycnals, lateral diffusion acts as an unrealistically large diapycnal diffusion in regions where there are steeply sloping isopycnals. Redi (1982) suggested a method of rotating the diffusion tensor (denoted ISO) which was implemented in the GFDL model by Cox (1987). Unfortunately, the scheme as implemented still requires a small lateral mixing for computational stability and so mixing is not exclusively along isopycnals. Gent and McWilliams (1990) further proposed a parameterization (denoted GM) of mesoscale eddy-induced mixing in terms of down-gradient isopycnal thickness diffusion, in addition to the diffusion along isopycnals. This thickness diffusion results in an additional 'bolus' transport velocity

$$\mathbf{u}^* = \frac{\partial}{\partial z}\left(k_t \frac{\nabla \rho}{\rho_z} \right) \quad , \quad w^* = -\nabla \cdot \left(k_t \frac{\nabla \rho}{\rho_z} \right) \qquad (11)$$

which is added to mean velocity in the tracer equations (Danabasoglu *et al.*, 1994). Here k_t is the isopycnal thickness diffusivity and $\mathbf{u}^*=(u^*,v^*)$ and w^* are the horizontal (x,y) and vertical (z) components of the bolus transport velocity, respectively.

3.1 Idealized basin model

In this section, the model used has a 3.5° latitude by 3.75° longitude horizontal grid, with a 4500 metres deep, flat-bottomed ocean. The domain is 60° wide, and extends from 0° to 70° in the south-north direction. At the equator a symmetry condition is used. In the vertical, 15 levels are used, with the thickness varying from 50 metres at the surface to 550 metres at the bottom.

The horizontal and vertical viscosity are set everywhere to 2.5×10^{5} m^2s^{-1} and 10^{-3} m^2s^{-1}, respectively. The vertical diffusivity is set to 10^{-4} m^2s^{-1}. The horizontal diffusivity will vary depending on the mixing scheme used. For the HOR scheme, the horizontal diffusivity is set to 2.0×10^{3} m^2s^{-1}. For the ISO scheme, it is set to 5.0×10^{2} m^2s^{-1}, and to zero in the GM scheme. In ISO and GM, the isopycnal diffusivity is set to 2.0×10^{3} m^2s^{-1} as is the thickness diffusivity in GM. The model was then run for 3000 years for the three schemes with the results being close to equilibrium at the end.

Starting with the 3000-year state (using HOR), the model was run for an additional 61 years, using the atmospheric surface boundary condition for CFCs shown in Figure 1, and the solubility equations from the previous section. The CFCs were introduced in the first level of the model using three different methods: restoring to C_{esw} using the same restoring time-scale as used by the surface temperature and salinity boundary condition (40 days -- Equation 8); using the Liss and Merlivat parameterization (Equation 5); or using the one proposed by Wanninkhof (Equation 6). The first method is similar to experiment #2 in England *et al.* (1994) while the third one is described as experiment #4 in the same paper (without a sea-ice cover dependence). For the second and third methods, the wind speeds used (for Equations 5 and 6) are derived from a bulk formula equation for wind stress. The wind stress forcing in this model is given by a simple analytic equation (Bryan, 1987). Figure 2 shows the zonally-averaged concentration of CFC-11 after 61 years for

the restoring case. The increase in CFC concentrations at the surface is higher in the northern latitudes due to inverse relation between CFC solubilities and water temperature. In the deep ocean, higher concentrations of CFCs are found in the northern part of the domain in regions of deep-water formation. Figures 3 to 5 show the differences between the CFC results for the three method. The restoring method gives the highest amount of CFCs in the northern part of the domain, followed by the Wanninkhof method, and last by the Liss and Merlivat method. It is difficult to say which method is better as the model wind is idealized and so a model-data intercomparison is no feasible. Nevertheless these results show that substantial differences in CFC-11 distributions can arise through the surface boundary conditions formulations.

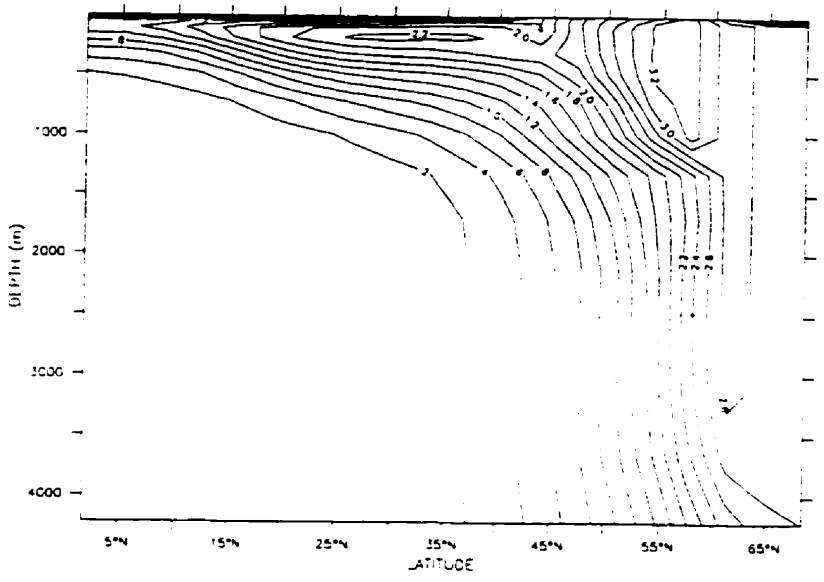

Figure 2. Zonally-averaged concentration of CFC-11 (pmol kg^{-1}) after 61 years in the restoring case.

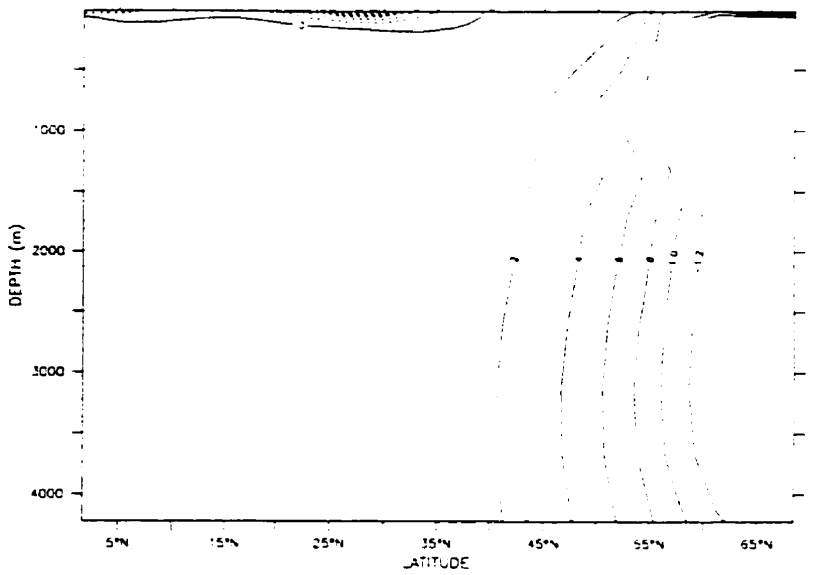

Figure 3. Zonally-averaged difference in concentration of CFC-11 (pmol kg^{-1}) between the Restoring and Liss & Merlivat methods.

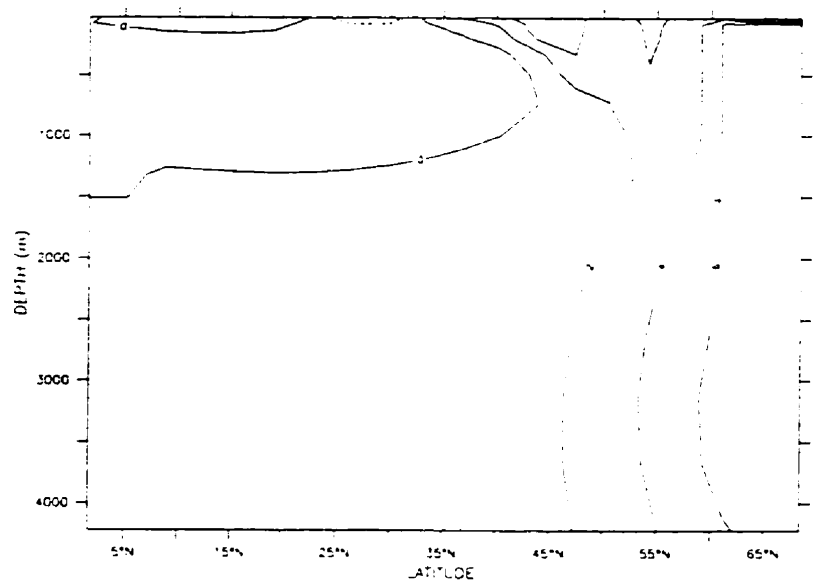

Figure 4. Zonally-averaged difference in concentration of CFC-11 (pmol kg^{-1}) between the Restoring and Wanninkhof methods.

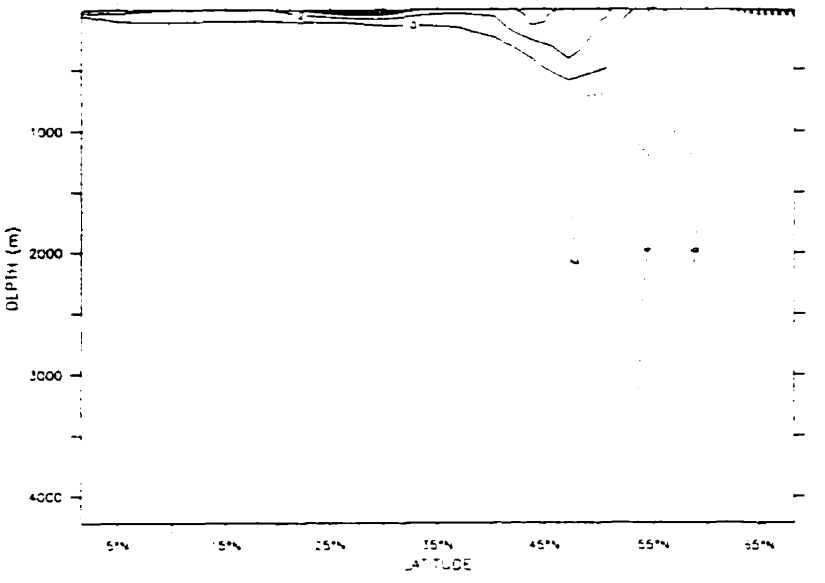

Figure 5. Zonally-averaged difference in concentration of CFC-11 (pmol kg^{-1}) between the Liss & Merlivat and Wanninkhof methods.

The differences between HOR, ISO and GM will now be examined by using only the restoring method for CFCs, and looking at zonally-averaged differences using the different sub-grid-scale mixing schemes. For ISO (Figure 6), the maximum in CFC-11 concentration occurs, as in the HOR case (Figure 2), at roughly 60°N, but is more larger in size, and influences the deep ocean more at this latitude than HOR. For GM (Figure 7), the maximum is more limited to the surface layer, and is more northward in the domain. The slope of the concentration lines are also different. In HOR, they are nearly vertical in most of the deep-ocean, while in GM, they are at 45°. ISO is located between these two cases. This section showed that various surface boundary conditions and sub-grid-scale mixing schemes give different results for CFC-11 concentrations. In the next section, the level of complexity of the ocean model used will be increased in the hope of obtaining more realistic results.

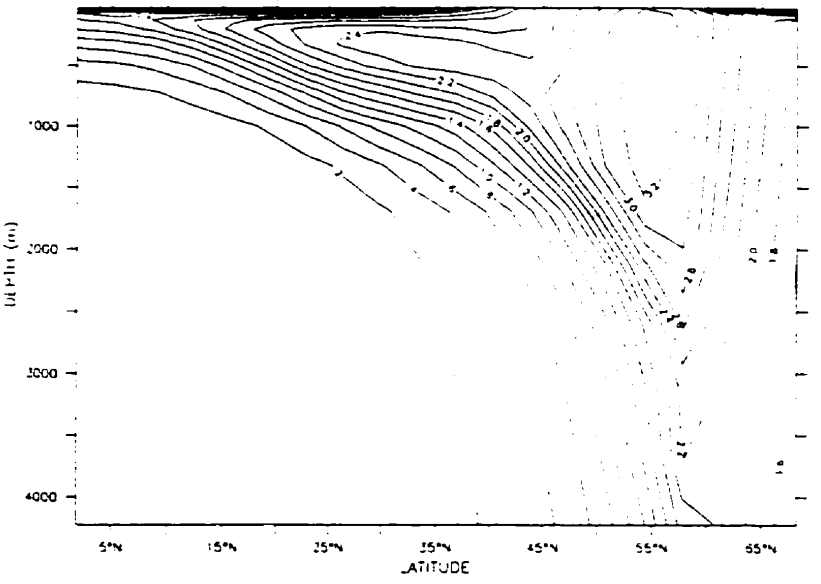

Figure 6. Zonally-averaged concentration of CFC-11 (pmol kg^{-1}) in the isopycnal case (ISO).

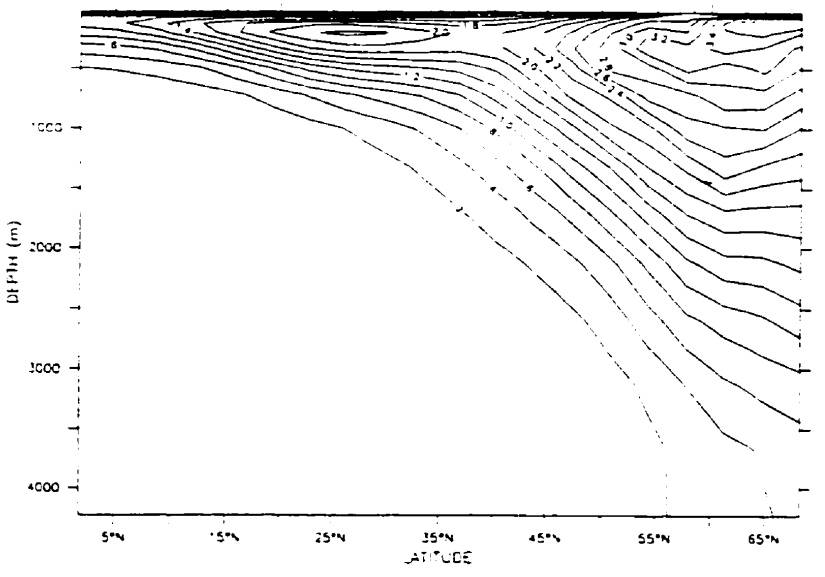

Figure 7. Zonally-Averaged concentration of CFC-11 (pmol kg^{-1}) in the Gent and McWilliams case (GM).

3.2 High resolution model of the North Atlantic

To test the influx of atmospheric CFCs into an ocean model in a more realistic scenario, a modified version of the Bryan-Cox model was used. This model covers the North Atlantic with 20 vertical levels (down to 4020 metres) and a horizontal resolution of 1° by 1°. The model was first run (without CFCs) for 953 years by restoring the surface temperatures and salinities to the annual mean values of Levitus (1982) and using the Hellerman and Rosenstein (1983) annual mean surface wind stress. Some of the parameters used by the model are shown in Table 4 and the topography of the model can be seen in Figure 8. The model uses the lateral/vertical mixing scheme (HOR).

Table 4. Parameters used in the high-resolution Bryan-Cox model in the 953-year run toward equilibrium.

Symbol	Description	Value
A_m	Lateral Eddy Viscosity	10^4 m^2s^{-1}
A_h	Lateral Eddy Diffusivity	10^3 m^2s^{-1}
K_m	Vertical Viscosity Coefficient	10^{-3} m^2s^{-1}
K_h	Vertical Diffusion Coefficient	10^{-4} m^2s^{-1}
Δt_{ts}	Time Step for Density and tracer	43200 seconds
Δt_{uv}	Time Step for baroclinic velocity	1800 seconds
Δt_{ψ}	Time Step for barotropic velocity	1800 seconds

Figures 9 and 10 show the barotropic and overturning streamfunction of the model. The maximum circulation in the horizontal is 36 Sv in the sub-tropical gyre, and 24 Sv in the subpolar gyre. In the vertical, the maximum overturning circulation reaches 13 Sv between 45 and 50°N. Figures 11 and 12 show the zonally-averaged temperature and salinity field for the model basin. When comparing the temperature field to observations of the North Atlantic (e.g., Levitus, 1982), it can be seen that the thermocline is too diffuse

with temperatures too high in the deep-ocean. The salinity field gives values more realistic compared to observations. Some of the problems with the temperature field maybe are due to the lack of communications with the Arctic and South Atlantic, and especially a lack of cold Antarctic bottom water entering the model.

The model was then integrated for 57 additional years using a realistic atmospheric forcing for CFC-11 to simulate the period from 1931 to 1988. Figure 13 shows the observations taken from Doney and Bullister (1992) in the eastern North Atlantic (between 20°W and 30°W) acquired in 1988, while Figure 14 shows the CFC-11 results in the model following the same cruise path. One can clearly see the progression of CFC 11 from the surface towards the deep-ocean in the north (where the region of deep-water formation is situated), and then toward the equator. When comparing observations to model output, it can be seen that the modeled results are similar in profile and magnitude. The same concentrations in deep-water in the model and the observations are roughly at the same location in the ocean. Also, the maximum concentrations at the surface are roughly at the same location (around 55° N). This seems to indicate that the model is doing a good job in reproducing the pattern in concentrations of CFC. Because of problems with the boundary conditions in this model (which for example give unrealistic values for the deep-ocean temperatures), a more sophisticated model will be used in the next section.

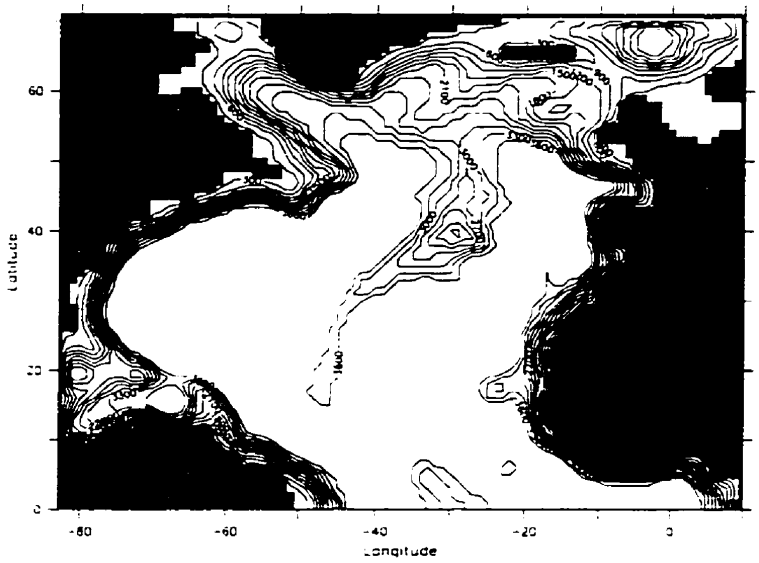

Figure 8. Topography of the high resolution model of the North Atlantic (in metres).

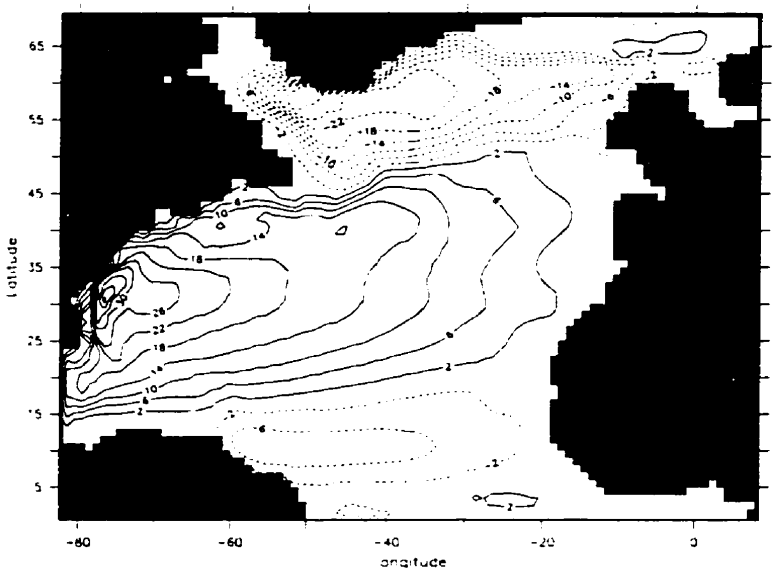

Figure 9. Barotropic streamfunction of the high resolution model (in Sverdrup).

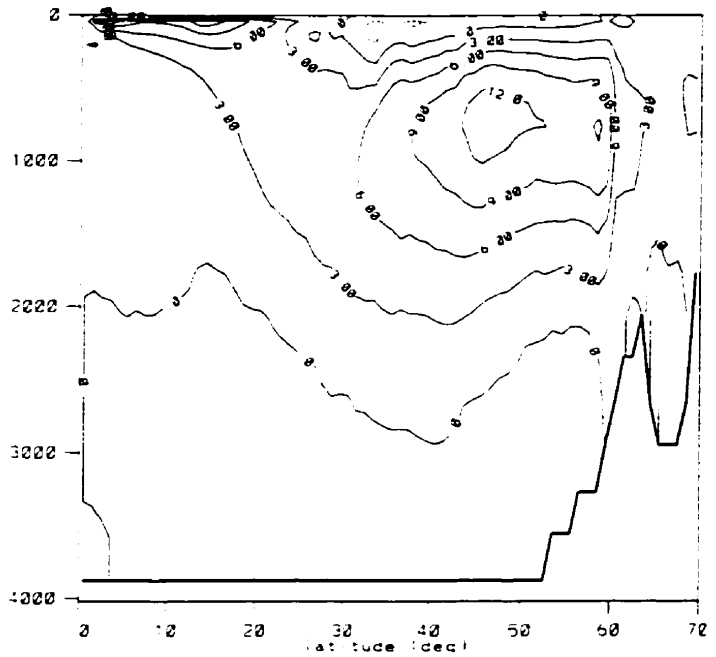

Figure 10. Meridional overturning streamfunction of the high resolution model (in Sverdrup).

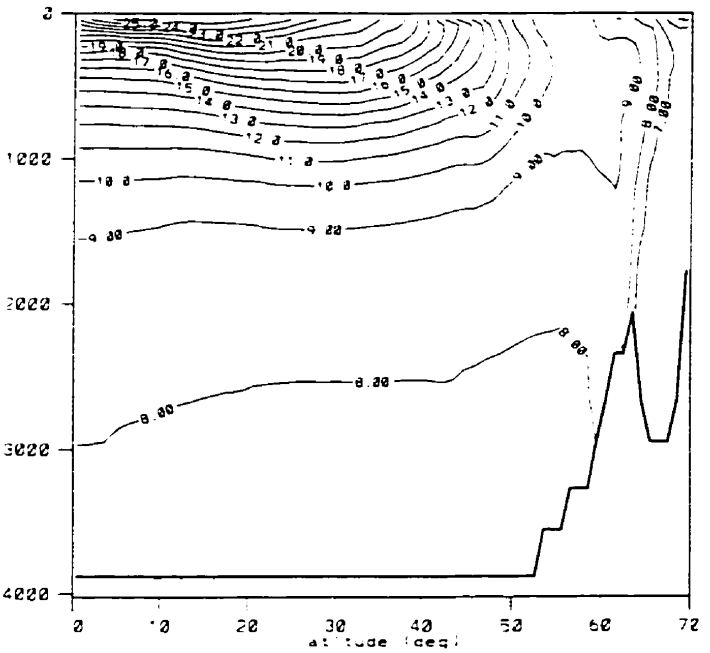

Figure 11. Zonally-averaged temperature (°C) in the high resolution model.

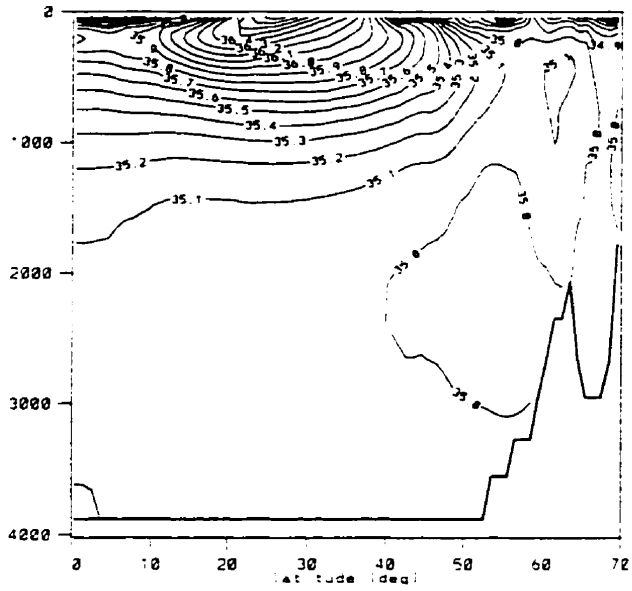

Figure 12. Zonally-averaged salinity of the high-resolution model.

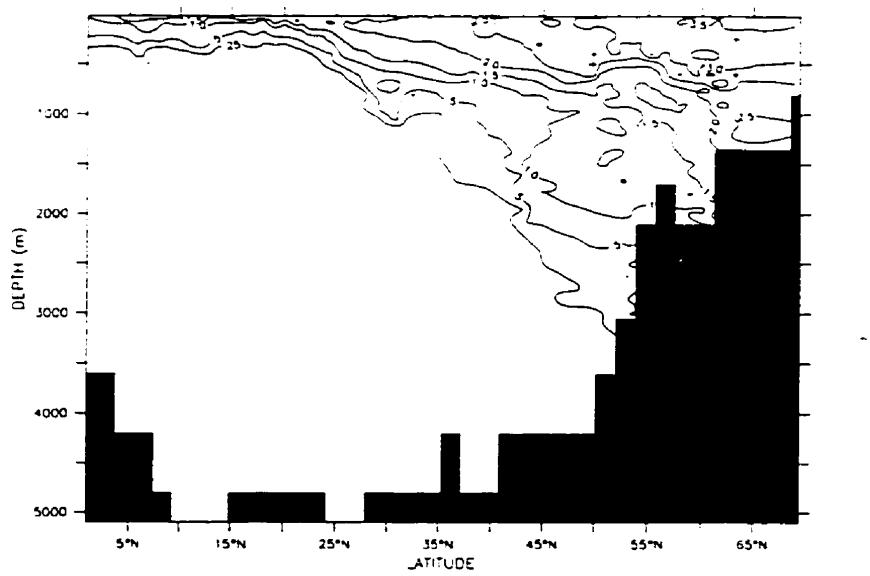

Figure 13. a)— Concentration of CFC-11 (pmol kg^{-1}) observed in July/August 1988 in the eastern North Atlantic on a cruise track varying between 20°W and 30°W (redrawn from Doney and Bullister, 1992). The topography is taken from the global model in section 3.3.

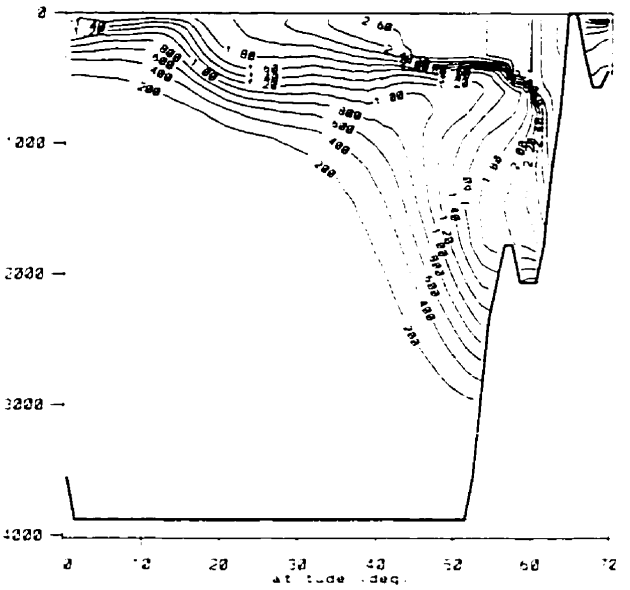

Figure 14. North Atlantic CFC-11 concentration (pmol kg $^{-1}$) for July 1988 in the high resolution model following the same cruise path as the observations shown in Figure 13.

3.3 Global model

Experiments similar to the idealized basin model in Section 3.1 will now be applied to a global model. The global model used in this section is a global version of the MOM ocean model described in Weaver and Hughes (1996). The resolution of the model is 3.75° x 1.8555° (latitude x longitude) with 19 vertical levels. The model was first integrated to equilibrium for 4000 years while restoring the surface temperatures and salinities to the annual mean values of Levitus (1982) with some small modifications in polar regions (see Weaver and Hughes, 1996). Hellerman and Rosenstein (1983) annual mean wind stress data and the lateral/vertical mixing scheme were also used in this run (denoted HOR). The model was further integrated for an additional 2000 years using the rotated diffusion tensor (this run is denoted ISO), as proposed by Redi (1982) and implemented in the GFDL model by Cox (1987). In the third experiment (denoted GM), the model was restarted from the end of HOR and continued the integration to equilibrium for 2000 years with the sub-grid-scale mixing scheme proposed by Gent and McWilliams (1990).

In all experiments, the horizontal and vertical viscosities were assigned values of $A_h = (2 + 2\cos\phi) \times 10^5\ m^2s^{-1}$ and $A_v = 2 \times 10^{-3}\ m^2s^{-1}$, respectively, where ϕ is the latitude. These numbers were chosen to be sufficiently large so as to avoid numerical noise. The vertical diffusivity in the three experiments was taken as

$$k_v = \left[0.61 + \pi^{-1}\tan^{-1}\left(1.5\times10^{-3}\left(z-10^3\right)\right)\right]\times10^{-4}\,m^2s^{-1} \qquad (12)$$

so that k_v varied from $3 \times 10^{-5}\ m^2s^{-1}$ at the surface to $1.1 \times 10^{-4}\ m^2s^{-1}$ at the bottom of the ocean (5400 metres).

The horizontal diffusivity in HOR was taken to be $k_h = 10^3\ m^2s^{-1}$. This was reduced to $10^2\ m^2s^{-1}$ in ISO (required for computational stability) and set to zero in GM. In GM and ISO the isopycnal diffusivity was chosen to be $k_i = 10^3\ m^2s^{-1}$ and the maximum isopycnal

slope (required for computational stability) in ISO to be 1/100. In GM, the values for k_l and k_t (isopycnal thickness diffusivity) are reduced toward zero when the slope becomes too large. Motivated by the work of Danabasoglu et al. (1994), k_t was chosen to be the same as k_l. All of the above coefficients are therefore consistent between the three experiments.

Very distinct model climatologies were obtained at the end of the HOR, ISO and GM integrations. Figures 15a-b show globally-averaged vertical potential temperature and salinity profiles for the three experiments and for the observations of Levitus and Boyer (1994) and Levitus *et al.* (1994). In the deep ocean, GM and ISO are colder than the observations, while HOR is warmer. For the salinity profile both ISO and GM show features similar to the observations, but GM is generally saltier and ISO generally fresher than the real ocean. The salinity curve of HOR does not capture the minimum at ~750m, and is too fresh in the deep ocean. The reason why GM is colder and saltier, and ISO is colder, than the observations in the deep ocean, is partially due to the surface boundary condition used in the polar regions. In these regions, the restoring boundary condition was artificially cooled and made saline (see Weaver and Hughes, 1996), to correct for the apparent fair-weather bias in the Levitus data set. This modification was done to tune the original climatology of HOR as best as possible and hence was clearly too strong a correction for the ISO and GM cases.

Figures 16 to 18 illustrate the meridional overturning streamfunction for HOR and ISO, and the effective meridional overturning streamfunction (mean meridional + bolus transport — see Danabasoglu et al., 1994) for GM. The maximum meridional overturning in the Northern Hemisphere is largest in ISO (15.6 Sv), followed by HOR (13.2 Sv) and GM (11.5 Sv). As in Danabasoglu et al. (1994), a large counterclockwise cell exists in HOR at the southern edge of the domain (32 Sv) with a Deacon Cell of 28 Sv. In ISO, the

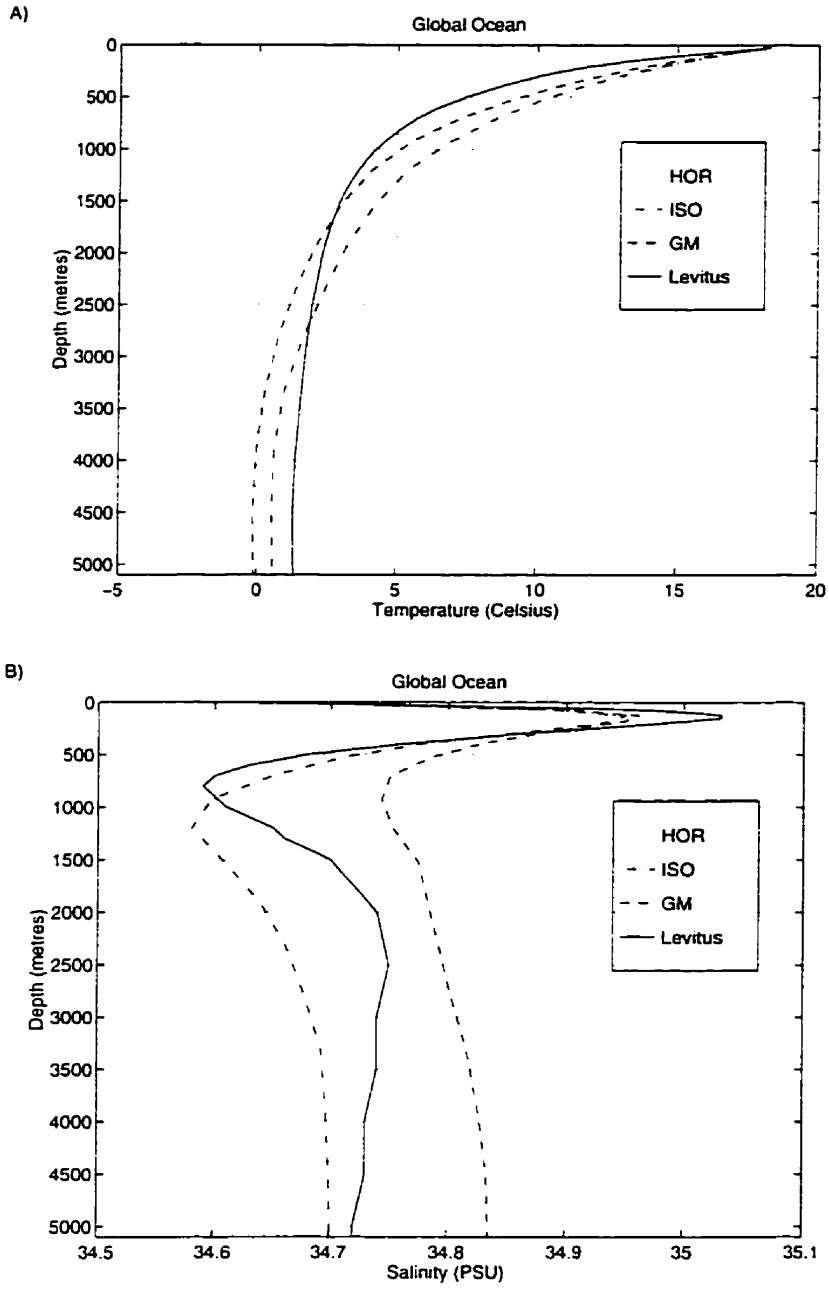

Figure 15. Temperature and salinity profiles for the three experiments and from observations of Levitus and Boyer (1994) and Levitus *et al.* (1994).

southern cell is reduced to 26 Sv, but the magnitude of the Deacon Cell stays roughly the same. With GM, the effective streamfunction (that which is relevant to the tracer continuity equation) shows a marked decrease in the southern cell (~20 Sv) and Deacon Cell (~16 Sv). This behaviour between HOR and GM is similar to the one described in Danabasoglu et al., 1994. In addition, our results suggest that the difference seen by Danabasoglu et al., 1994 is mainly due to the bolus transport component of their scheme (Equation 11) instead of the isopycnal mixing component of the scheme.

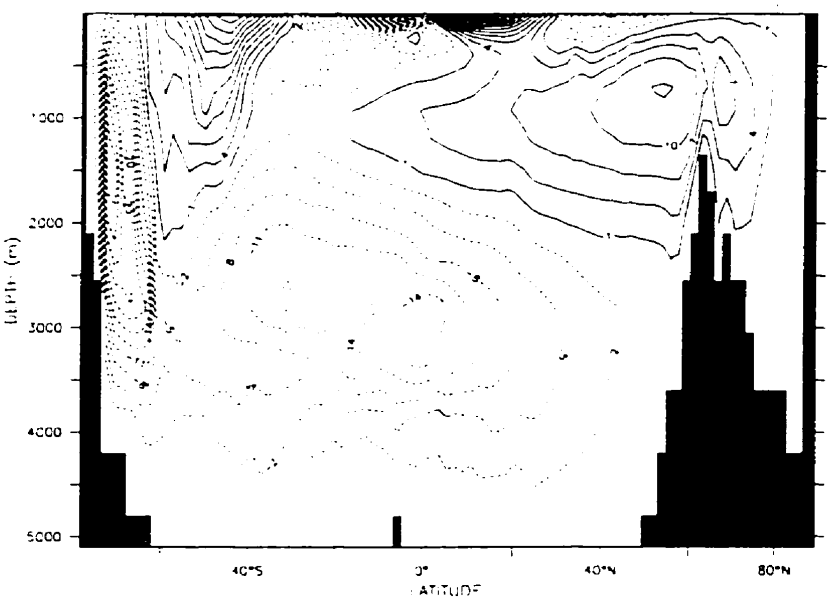

Figure 16. Meridional overturning streamfunction in HOR.

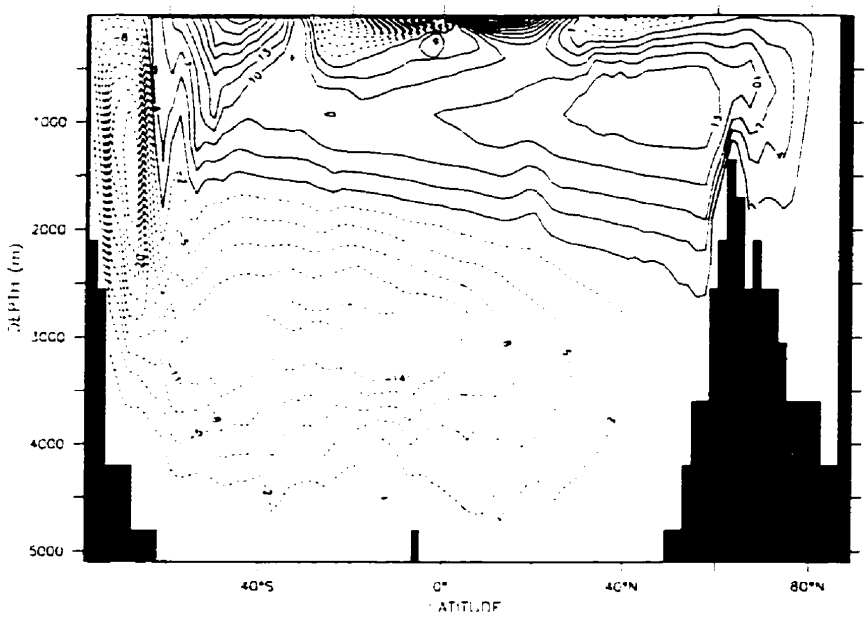

Figure 17. Meridional overturning streamfunction in ISO.

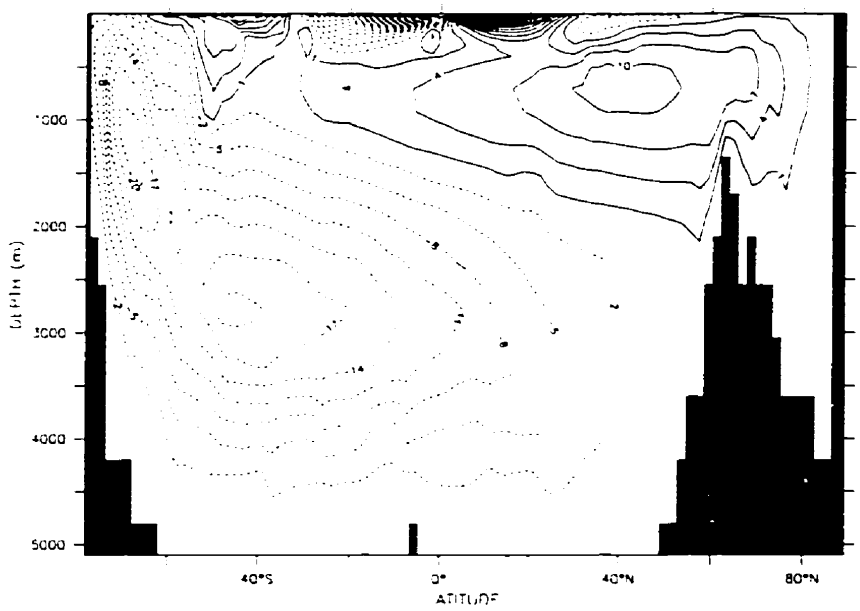

Figure 18. Effective meridional overturning streamfunction in GM.

The northward heat transport for the global and Atlantic oceans are plotted in Figures 19 and 20. Both the ISO and GM runs reveal a substantial decrease in the heat transport across the Antarctic Circumpolar Current consistent with the eddy-resolving model simulations discussed in Covey (1994). This result is due to the substantial reduction in lateral diffusion associated with the rotation of the diffusion tensor. In the Northern Hemisphere, the maximum transport is greatest in ISO (1.44 pW), followed by GM (1.33 pW) and HOR (1.13 pW), while in the Atlantic Ocean the maximum northward heat transport in ISO, GM and HOR is 0.91 pW, 0.74 pW, and 0.64 pW, respectively. The reduction of heat transport in GM compared to ISO is a result of the reduced effective overturning in the North Atlantic associated with GM.

In order to compare the ocean model under the three different sub-grid-scale parameterizations, three 60-year integrations were carried out (from 1931 to 1991) using the observed atmospheric CFC-11, as done in the previous section. This was done using the Liss and Merlivat method to calculate a CFC flux between the ocean and the atmosphere. In addition, in ice-covered regions, the gas transfer velocity for CFC-11 is reduced using $\lambda_i = \lambda(1 - F/10)$, where F is the fraction of sea-ice cover in tenths (0 = no ice; 10 = complete ice cover). An annual mean ice cover climatology was obtained from the monthly ice concentrations of Gloersen *et al.* (1992).

The Liss and Merlivat method could very well give too low a gas exchange rate (Sarmiento *et al.*, 1992), but the same paper also shows that a 100% increase in gas exchange rate in their OGCM only increases the cumulative oceanic uptake of CO_2 by 9.2%. This suggests any reasonable gas exchange scheme would only vary the total uptake by a few percent.

Figure 21a shows the CFC-11 observations that were taken in the eastern North Atlantic during July/August 1988 (Doney and Bullister, 1992). Figures 21b-d show the

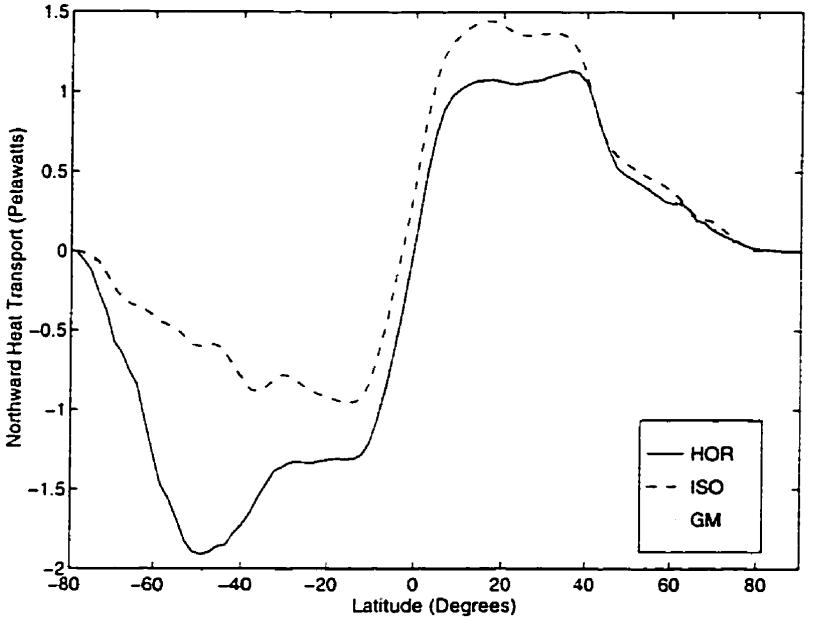

Figure 19. Global northward heat transport in petawatts for the three sub-grid-scale parameterizations in the global ocean model.

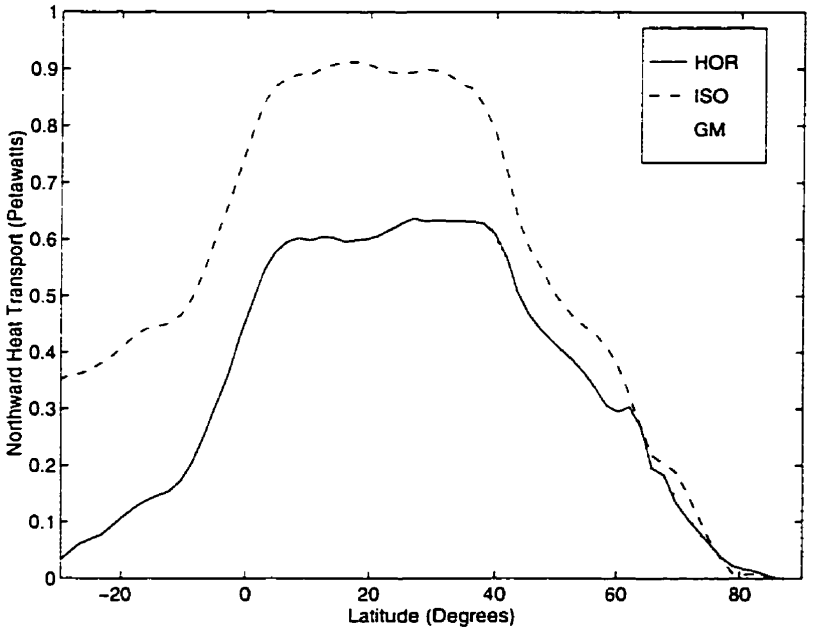

Figure 20. North Atlantic northward heat transport in petawatts for the three sub-grid-scale parameterizations in the global ocean model.

CFC-11 concentration in HOR, ISO, and GM along the same cruise path. Figures 22b-d show the differences in CFC-11 concentration between the HOR, ISO, and GM and observations along the same cruise path. The three schemes show surface values that are very close to the observations, which indicates that our parameterization of the air-sea exchange of CFC-11 is reasonable. This close match breaks down north of 65°N, probably because the ice cover in the annual-mean model remains constant and hence is different from the actual ice cover at the time of the observations. For the three schemes, too much CFC-11 is present in the upper 1000 m of the model, especially near the equator, which suggests that the vertical diffusivity (k_v) is too high in these regions. At the northern boundary, from the surface to about 1500 m, he concentrations using the three schemes are too high, with GM being the best of the three. Both HOR and GM exhibit a region of too low concentration of CFC-11 at ~500 m north of 45°N. The fact that ISO is overestimating the transport of CFC-11 can be seen by the pool of higher concentration CFC-11 at ~2000 m near the equator. This water comes from NADW (North Atlantic Deep Water) which flows along on the western boundary before crossing the cruise path near the equator.

In the Southern Hemisphere, using observations (Figure 23a) taken in late 1983/early 1984 (Warner and Weiss, 1992) we also see too much CFC-11 in the surface water above ~1000 m (Figure 24b–d). South of the ridge at 55°S, the deep ocean CFC concentration is too high in HOR, which is not the case in either ISO or GM. ISO, however, does a worse job than the other two experiments in waters shallower than ~2000 m.

A useful method to determine which mixing scheme gives the best simulated CFC-11 distribution, when compared to the observations, is to look at the rms differences for each cruise path and each scheme. The overall performance of the three experiments was calculated using the relation:

$$X = \frac{\sum(\text{Model - Observations})^2}{\sum(\text{Observations})^2}. \qquad (13)$$

This relation was summed over a regular and equal area grid onto which the observations and model output were interpolated. In the Northern Hemisphere, the grid extends from 5°S to 70°N, with an interval of 0.6°, while in the vertical it extends from the surface to 5100 m in 25 m intervals. In the Southern Hemisphere, the same vertical grid was used, but in the meridional direction the 0.6° spacing went from 70°S to 0°. For the North Atlantic, this analysis yielded X=0.214, 0.210, and 0.147 for HOR, ISO and GM, respectively. For the South Atlantic, the results for the same three experiments were X=1.52, 1.59, and 0.816, respectively. This indicates that over both these two sections the GM scheme gives significantly better results than both HOR and ISO, with most of the improvement occurring in the intermediate and deep ocean.

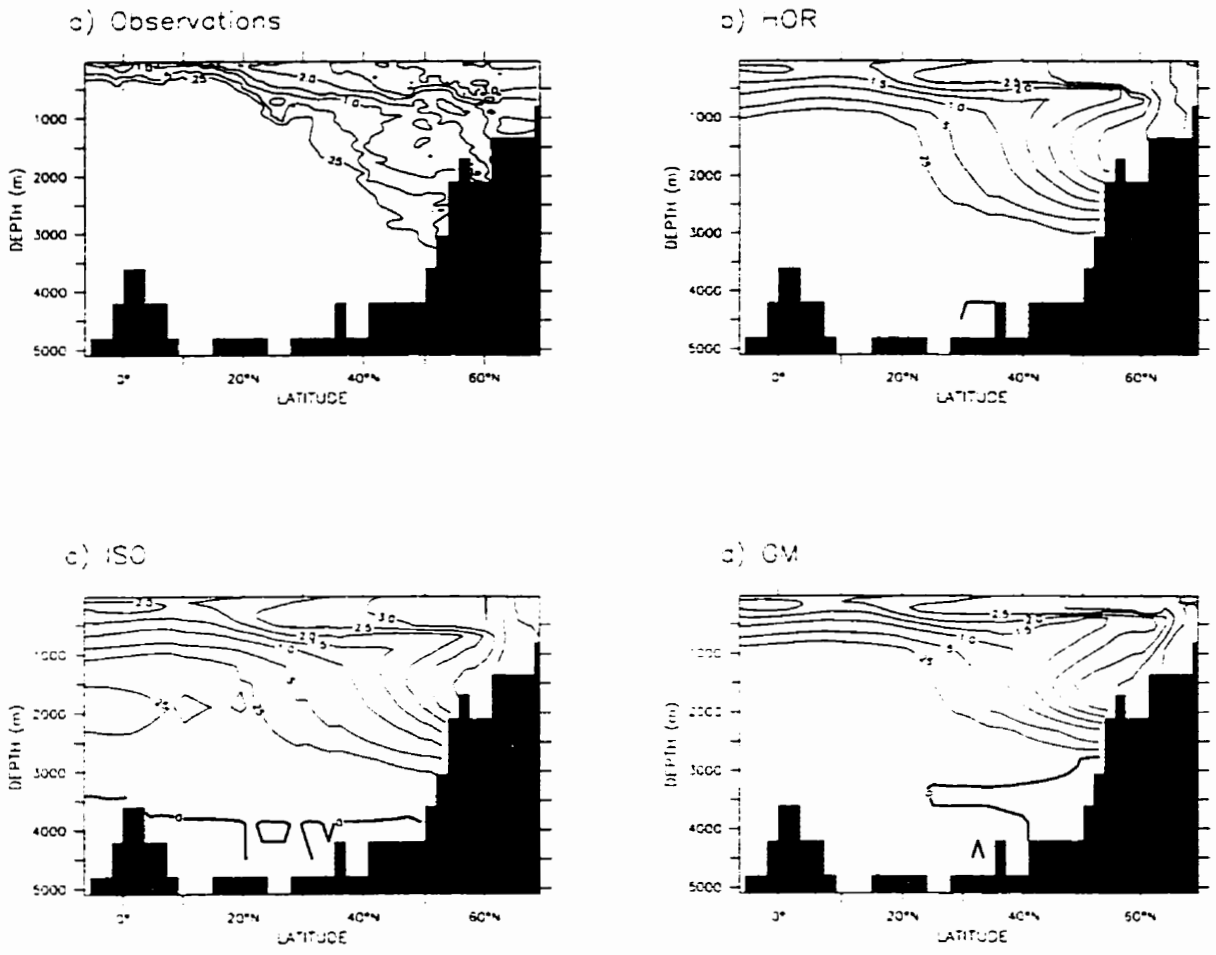

Figure 21. a)— Concentration of CFC-11 (pmol kg^{-1}) observed in July/August 1988 in the eastern North Atlantic on a cruise track varying between 20°W and 30°W (redrawn from Doney and Bullister, 1992). b)— Concentration of CFC-11 (pmol kg^{-1}) in HOR along the same cruise track. c)— same as b) but for ISO; d)— same as b) but for GM.

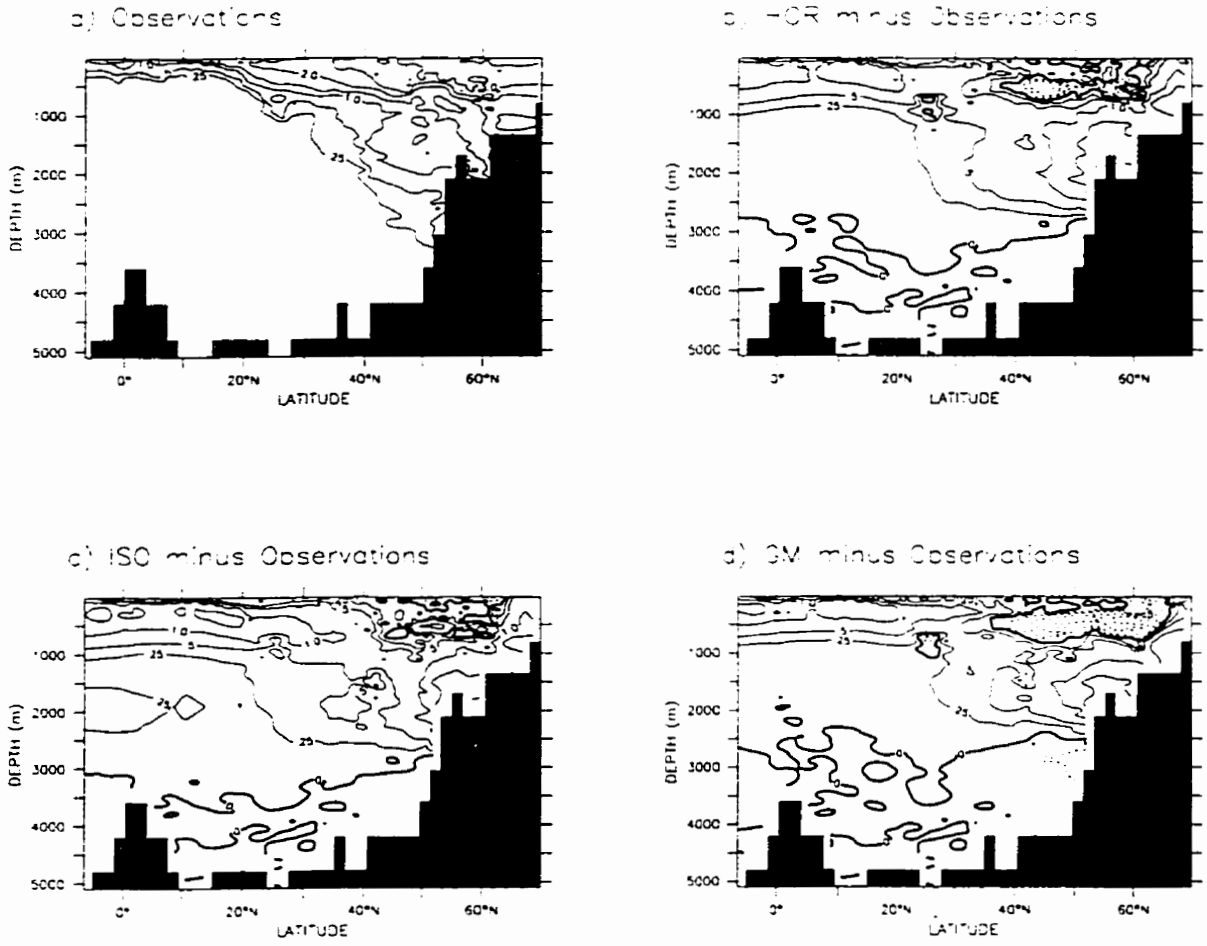

Figure 22. a)— Concentration of CFC-11 (pmol kg^{-1}) observed in July/August 1988 in the eastern North Atlantic on a cruise track varying between 20°W and 30°W (redrawn from Doney and Bullister, 1992). b)— Concentration of CFC-11 (pmol kg^{-1}) in HOR minus observations from a) along the same cruise track. c)— same as b) but for ISO; d)— same as b) but for GM.

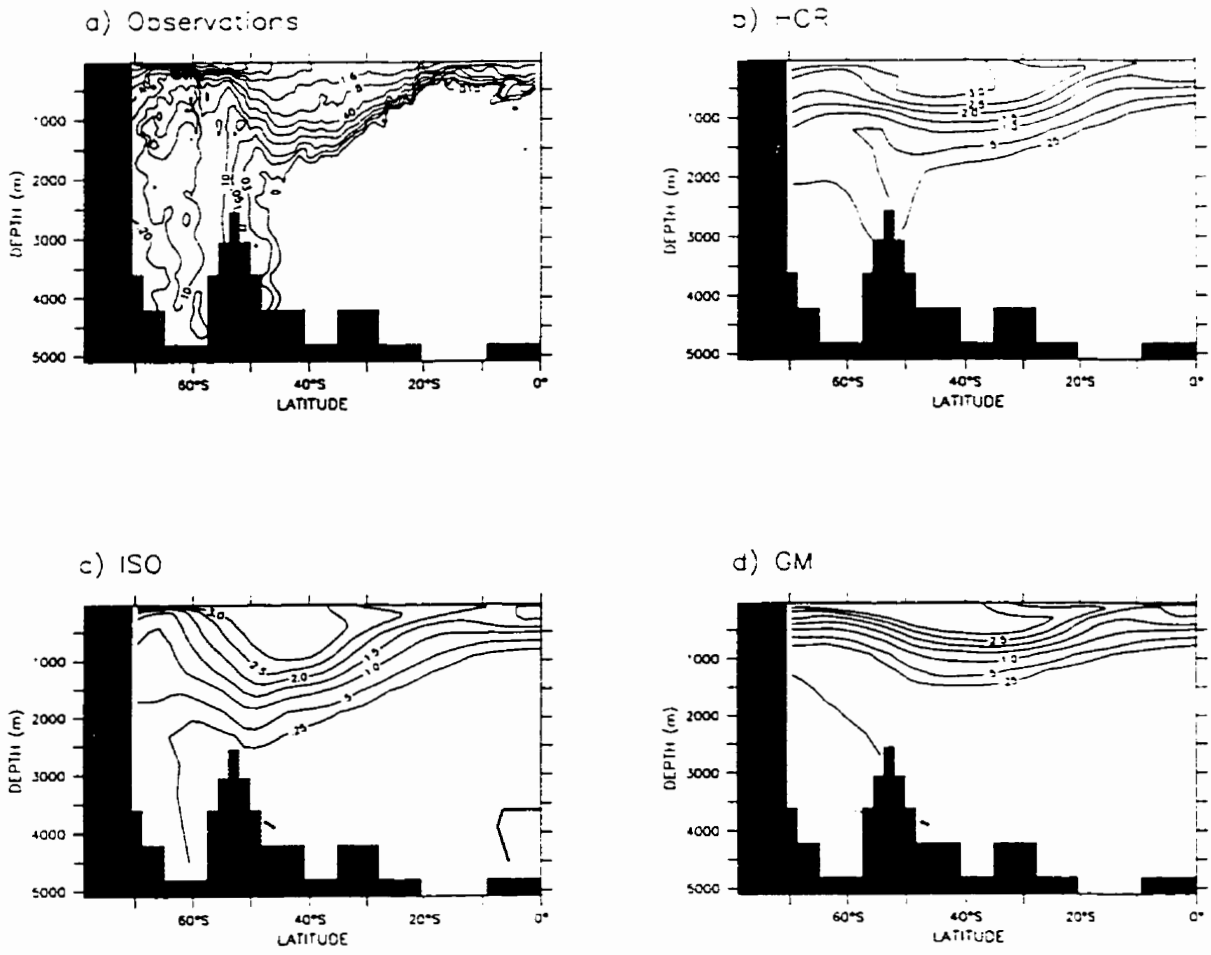

Figure 23. a)— Concentration of CFC-11 (pmol kg^{-1}) observed in October 1983 and January 1984 during the Ajax program along the prime meridian (taken from Warner and Weiss, 1992). b)— Concentration of CFC-11 (pmol kg^{-1}) in HOR. c)— same as b) but for ISO; d— same as b) but for GM.

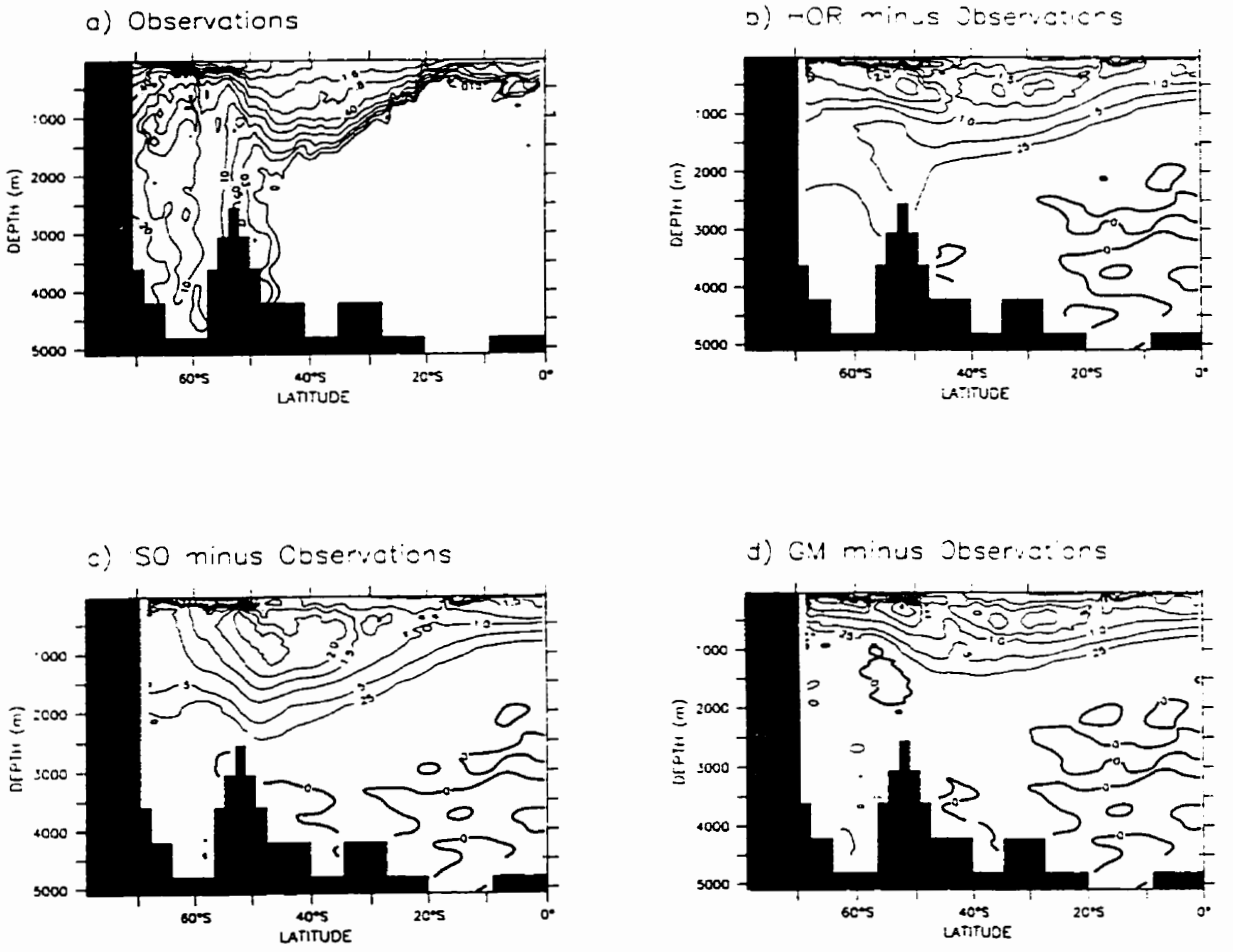

Figure 24. a)— Concentration of CFC-11 (pmol kg^{-1}) observed in October 1983 and January 1984 during the Ajax program along the prime meridian (taken from Warner and Weiss, 1992). b)— Concentration of CFC-11 (pmol kg^{-1}) in HOR minus observations from a). c)— same as b) but for ISO; d— same as b) but for GM.

4. Summary and conclusions

In this thesis, CFCs were used as a passive tracer in various numerical models, ranging from a simple basin model to a global model. First, a summary on how to introduce CFCs in an ocean model was given, with details on historical atmospheric concentrations, air-sea gas exchange rates, and a method to introduce atmospheric CFCs in a numerical ocean model.

Then the results from different kinds of numerical models were presented: first from a basin model; then in a high-resolution North Atlantic model; and finally from a global model. In the first and last case, three different kinds of sub-grid-scale mixing schemes were used: a lateral/vertical scheme; an isopycnal scheme (from Redi 1982); and the Gent and McWilliams scheme (Gent and McWilliams, 1990). Also, in the basin model, the effect of two different methods to find air-sea gas exchange coefficients was examined. The two methods gave different concentrations in the deep-ocean, a result also seen in a global model (Dixon *et al.*, 1996). In an effort to get more realistic results, and to be able to compare in a more realistic fashion model outputs to observations, the complexity of the models used was increased from the basin model, to the high-resolution North Atlantic model, and finally to a global model.

I will now look briefly at some of the results in the global model when changing sub-grid-scale mixing schemes. When the diffusion tensor was rotated (ISO), the deep ocean potential temperatures and salinities were greatly improved over those obtained with lateral/vertical mixing (HOR). Ironically, the CFC-11 distribution was no better with the inclusion of the isopycnal mixing parameterization. The use of the Gent and McWilliams scheme, on the other hand, substantially improved the CFC-11 distributions (especially in the southern Atlantic) and upper ocean potential temperature. The former improvement is

associated with the elimination of the Deacon Cell which caused too much vertical penetration of CFC in the southern hemisphere.

Recent results from transient experiments conducted to look at the climatic response to increasing greenhouse gases (Washington and Meehl, 1989; Manabe et al., 1991; Cubasch et al., 1992; Murphy and Mitchell, 1995) have revealed an asymmetric response between the northern and southern hemispheres. Over the Southern Ocean these experiments have revealed relatively little short term warming (or even cooling) due to the efficient absorption of heat in this region. All of the ocean components of these coupled atmosphere-ocean GCMs have used either lateral/vertical or isopycnal sub-grid-scale mixing schemes. The results in section 3.3 have shown that these schemes significantly overestimate the CFC uptake of the ocean in the southern hemisphere due to the existence of the Deacon Cell. This could suggest that the heat uptake may also be overestimated in these models thus reducing the climatic response to increasing greenhouse gases, although experiments with fully coupled models are required to verify this claim (e.g., Hirst *et al.*, 1996). The use of the Gent and McWilliams scheme appears to be a definite improvement, from a CFC-11 uptake point of view, in a global model, but in light of some recent results (Weaver and Eby, 1996), some numerical problems with the way the Gent and McWilliams scheme was implemented in this research will have to be addressed.

Also more work should be done to improve the precision of the air-sea gas exchange rate used for CFC in this thesis. In addition, the global model used in section 3.3 could be improved by using better resolution, better surface boundary conditions, and by the addition of a seasonal cycle. With a better ocean model, and a better surface CFC flux into the ocean model we would be able to look more closely at the weaknesses and strength of these kinds of ocean models from a CFC tracer point of view.

In conclusion, work in this thesis has shown that passive tracers like CFC-11 make an useful tool in evaluating results from oceanic models, and could be easily extended to other passive tracers like CFC-12, or CFC-113 depending on the observations.

References

Bryan, F. (1987): Parameter Sensitivity of Primitive Equation Ocean General Circulation Models. Journal of Physical Oceanography, **17**:970-985.

Bryan, K. (1969): A Numerical Method for the Study of the Circulation of the world Ocean. Journal of Computational Physics, **4**:347-376.

Bullister, J.L., and R.F. Weiss (1983): Anthropogenic Chlorofluoromethanes in the Greenland and Norwegian Seas. Science, **221**:265-268.

Butler, J.H., J.W. Elkins, T.M. Thompson, B.D. Hall, T.H. Swanson, and V. Koropalov (1991): Oceanic Consumption of CH_3CCl_3: Implications for Troposheric OH. Journal of Geophysical Research, **96**:22347-22355.

Cicerone, R.J., R.S. Stolarski, and S. Walters (1974): Stratospheric Ozone Destruction by Man-Made Chlorofluoromethanes. Science, 185:1165-1167.

Covey, C., (1994): Global Ocean Circulation and Equator-Pole Heat Transport as a Function of Ocean GCM Resolution. PCMDI Report No. 19, Lawrence Livermore National Laboratory, Livermore, CA.

Cox, M.D. (1987): Isopycnal Diffusion in a Z-Coordinate Model. Ocean Modelling, 74:1-5.

Cox, M.D. (1984): A Primitive Equation, Three-Dimentional Model of the Ocean. GFDL Ocean Group Technical Report No. 1.

Cubasch, U., K. Hasslemann, H. Höck, E. Maier–Reimer, U. Mikolajewicz, B. D. Santer, and R. Sausen (1992): Time-dependent greenhouse warming computation with a coupled atmosphere-ocean model, Climate Dynamics, **8**:55–69.

Cunnold, D.M., R.G. Prinn, R.A. Rasmussen, P.G. Simmonds, F.N. Alyea, C.A. Cardelino, A.J. Crawford, P.J. Fraser, and R.D. Rosen (1986): Atmospheric Lifetime and Annual Release Estimate for $CFCl_3$ and CF_2Cl_2 From 5 Years of ALE Data. Journal of Geophysical Research, **91**:10797-10817.

Danabasoglu, G., J. C. McWilliams, and P. R. Gent (1994): The Role of Mesoscale Tracer Transport in the Global Ocean Circulation, Science, **264**:1123-1126.

Dixon, K.W., J.B. Bullister, R.H. Gammon, and R.J. Stouffer (1996): Examining a Coupled Climate Model Using CFC-11 as an Ocean Tracer, Geophysical Research Letters, **23**:1957-1960.

Doney, S.C., and J.L. Bullister (1992): A Chlorofluorocarbon Section in the Eastern North Atlantic. Deep-Sea Research, **39**:1857-1883.

England, M.H. (1995): Using Chlorofluorocarbons to Assess Ocean Climate Models. Geophysical Research Letter, **22**:3051-3054.

England, M.H., V. Garçon, and J-F. Minster (1994): Chlorofluorocarbon Uptake in a World Ocean Model, 1. Sensitivity to the Surface Gas Forcing. Journal of Geophysical Research, **99**:25215-25233.

Gammon, R.H., J. Cline, and D. Wisegarver (1982): Chlorofluoromethanes in the Northeast Pacific Ocean: Measured Vertical Distributions and Application as Transient Tracers of Upper Ocean Mixing. Journal of Geophysical Research, **87**:9441-9454.

Gent, P. R. and J. C. McWilliams (1990): Isopycnal Mixing in Ocean Circulation Models, Journal of Physical Oceanography, **20**:150-155.

Gloersen, P., W. J. Campbell, D. J. Cavalieri, J. C. Comiso, C. L. Parkinson, and H. J. Zwally (1992): Arctic and Antarctic Sea Ice, 1978-1987: Satellite Passive-Microwave Observations and Analysis, Report SP-511, 290 pp., NASA, Washington, D.C.

Hahne, A., A. Volz, D.H. Ehhalt, H. Cosatto, W. Roether, W. Weiss, and B. Kromer (1978): Depth Profiles of Chlorofluoromethanes in the Norwegian Sea. Pure and applied Geophysics, **116**:575-582.

Hart, H. and J.-M. Conia (1987): Introduction à la chimie organique, InterEditions, Paris, 567p.

Hellerman, S., and M. Rosenstein (1983): Normal Monthly Wind Stress Over the World Ocean with Error Estimated, Journal of Physical Oceanography, **13**:1093-1104.

Hirst, A.C., H.B. Gordon, and S.P. O'Farrell (1996): Response of a Coupled Ocean-Atmosphere Model Including Oceanic Eddy-Induced Advection to Anthropogenic CO_2 increase, Geophysical Research Letters, submitted.

Hunter-Smith, R.J., P.W. Balls, and P.S. Liss (1983): Henry's Law Constants and Air-Sea Exchange of Various Low Molecular Weight Halocarbons Gases, Tellus, **35B**:170-176.

Levitus, S. (1982): Climatological Atlas of the World Ocean, NOAA Prof. Paper 13, 173 pp.,US Govt. Printing Office, Washington, DC.

Levitus S., and T. P. Boyer (1994): World Ocean Atlas 1994 Volume 4: Temperature, NOAA Atlas NESDIS 4, 117 pp., NODC, Washington, DC.

Levitus S., R. Burgett and T. P. Boyer (1994): World Ocean Atlas 1994 Volume 3: Salinity, NOAA Atlas NESDIS 3, 99 pp., NODC, Washington, DC.

Liss, P.S., and L. Merlivat (1986): Air-Sea Gas Exchange Rates: Introduction and Synthesis, in The Role of Air-Sea Echange in Geochemical Cycling, P. Buat-Menard (ed.), D. Reidel Publishing Company, Hingham, Mass., pp. 113-127.

Lovelock, J.E., R.J. Maggs, and R.J. Wade (1973): Halogenated Hydrocarbons in and over the Atlantic. Nature, **241**:194-196.

Manabe, S., R. J. Stouffer, M. J. Spelman, and K. Bryan (1991): Transient Responses of a Coupled Ocean-Atmosphere Model to Gradual Changes of Atmospheric CO_2. Part I: Annual Mean Response, Journal of Climate, **4**:785–818.

Murphy, J. M., and J. F. B. Mitchell (1995):, Transient Response of the Hadley Centre Coupled Ocean-Atmosphere Model to Increasing Carbon Dioxide. Part II: Spatial and Temporal Structure of Response, Journal of Climate, **8**:57–80.

Pacanowski, R., K. Dixon and A. Rosati, (1993): The G.F.D.L Modular Ocean Model Users Guide, GFDL Ocean Group Technical Report #2.

Redi, M.H. (1982): Oceanic Isopycnal Mixing by Coordinate Rotation. Journal of Physical Oceanography, **12**:1154-1158.

Rhein, M. (1991): Ventilation Rates of the Greenland and Norwegian Seas Derived from Distribution of the Chlorofluoromethanes F11 and F12. Deep-Sea Research, **38**:485-503.

Robitaille, D.Y., and A.J. Weaver (1995): Validation of Sub-Grid-Scale Mixing Schemes using CFCs in a Global Ocean Model. Geophysical Research Letters, **22**:2917-2920.

Roether, W., V.M. Roussenov, and R. Well (1994): A Tracer Study of the Thermocline Circulation of the Eastern Mediterranean, in: Ocean Processes in Climate Dynamics: Global and Mediterranean Examples. P. Malamotte-Rizzoli and A.R. Robinson (Eds.), Kluwer Acad. Pub., p. 371-394.

Sarmiento, J.L., J.C. Orr, and U. Siegenthaler (1992): A Pertubation Simulation of CO_2 Uptake in an Ocean General Circulation Model. Journal of Geophysical Research, **97**: 3621-3645.

Schlosser, P., G. Bönisch, M. Rhein, and R. Bayer (1991): Reduction of Deepwater Formation in the Greenland Sea during the 1980s: Evidence from Tracer Data. Science, **251**:1054-1056.

Semtner, A.J. (1986): Finite-Difference Formulation of a World Ocean Model. In: *Advanced Physical Oceanographic Numerical Modelling*, O'Brien, J.J., ed., NATO ASI Series, **186**, Reidel, 187-202.

Smethie, W.M. Jr., D.W. Chipman, J.H. Swift, and K.P. Koltermann (1988): Chlorofluoromethanes in the Arctic Mediterranean Seas: Evidence for Formation of Bottom Water in the Eurasian Basin and Deep-Water Exchange Through Fram Strait. Deep-Sea Research, **35**:347-369.

Trumbore, S.E., S.S. Jacobs, and W.M. Smethie Jr (1991): Chlorofluorocarbon Evidence for Rapid Ventilation of the Ross Sea. Deep-Sea Research, **38**:845-870.

Wallace, D.W.R., and R.M. Moore (1985): Vertical Profiles of CCl_3F (F-11) and CCl_2F2 (F-12) in the Central Arctic Ocean Basin. Journal of Geophysical Research, **90**:1155-1166.

Wanninkhof, R. (1992): Relationship Between Wind Speed and Gas Exchange Over the Ocean. Journal of Geophysical Research, **97**:7373-7382.

Warner, M.J., and R.F. Weiss (1992): Chlorofluoromethanes in South Atlantic Antarctic Intermediate Water. Deep-Sea Research, **39**:2053-2075.

Warner, M.J., and R.F. Weiss (1985): Solubilities of chlorofluorocarbons 11 and 12 in Water and Seawater. Deep-Sea Research, **32**:1485-1497.

Washington, W. M. and G. A. Meehl (1989): Climate Sensitivity Due to Increased CO_2: Experiments with a Coupled Atmosphere and Ocean General Circulation Model, Climate Dynamics, **4**:1–38..

Weaver, A.J., and M. Eby (1996): On the Numerical Implementation of Advection Schemes for use in Conjunction with Various Mixing Parameterizations in the GFDL Ocean Model, Journal of Physical Oceanography, in press.

Weaver, A. J., and T. M. C Hughes (1996): On the Incompatibility of Ocean and Atmosphere Models and the Need for Flux Adjustments, Climate Dynamics, **12**:141-170.

Wisegarver, D.P., and J.D. Cline (1985): Solubility of Trichlorofluoromethane (F-11) and Dichlorodifluoromethane (F-12) in Seawater and its Relationship to Surface Concentrations in the North Pacific, Deep-Sea Research, **32**:97-106.

Appendix

Table A-1. Atmospheric concentration of CFC-11 (in ppt, parts per trillion) between 1931 and 1991 in the Northern and Southern Hemispheres (R.F. Weiss, 1993, personal communication).

Year	Northern Hemisphere	Southern Hemisphere	Year	Northern Hemisphere	Southern Hemisphere
	(ppt)	(ppt)		(ppt)	(ppt)
1931	0.000	0.000	1962	14.601	11.781
1932	0.000	0.000	1963	17.766	14.235
1933	0.000	0.000	1964	21.601	17.271
1934	0.000	0.000	1965	26.091	20.919
1935	0.000	0.000	1966	31.103	25.141
1936	0.000	0.000	1967	36.642	29.900
1937	0.000	0.000	1968	42.940	35.265
1938	0.000	0.000	1969	50.114	41.349
1939	0.007	0.003	1970	58.505	48.349
1940	0.012	0.007	1971	67.959	56.352
1941	0.016	0.011	1972	78.160	65.254
1942	0.020	0.015	1973	89.740	75.188
1943	0.025	0.019	1974	103.061	86.455
1944	0.036	0.026	1975	117.451	99.000
1945	0.045	0.034	1976	130.468	111.784
1946	0.061	0.045	1977	143.764	124.542
1947	0.095	0.065	1978	156.000	136.946
1948	0.170	0.107	1979	166.979	148.548
1949	0.298	0.186	1980	176.942	159.210
1950	0.505	0.319	1981	186.405	169.098
1951	0.794	0.519	1982	193.003	177.486
1952	1.193	0.804	1983	201.961	185.570
1953	1.769	1.210	1984	210.370	193.368
1954	2.538	1.771	1985	219.499	202.921
1955	3.458	2.489	1986	230.869	211.689
1956	4.591	3.380	1987	240.132	219.597
1957	5.995	4.484	1988	250.439	230.740
1958	7.495	5.763	1989	256.248	239.826
1959	8.769	7.052	1990	263.553	248.222
1960	10.107	8.332	1991	265.704	254.148
1961	12.060	9.844			

IMAGE EVALUATION TEST TARGET (QA-3)

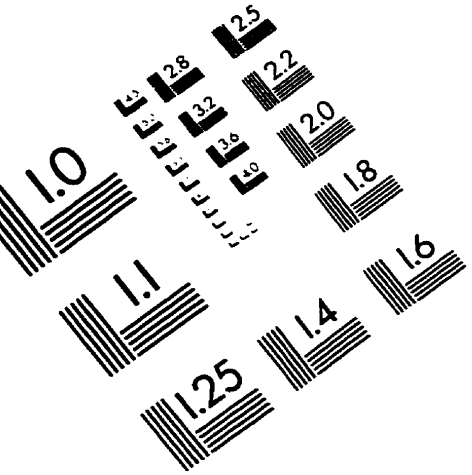

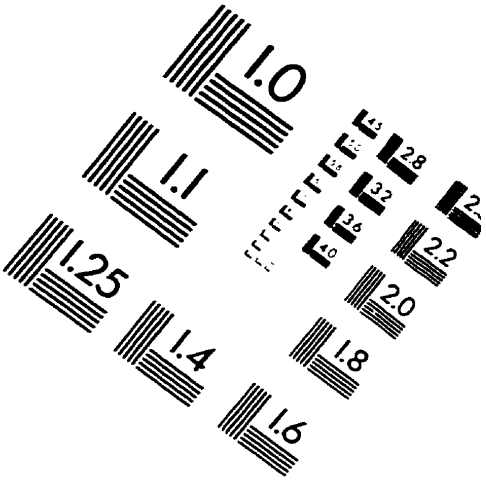

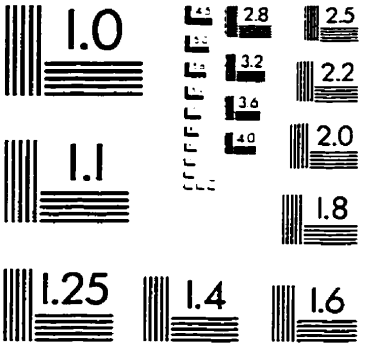

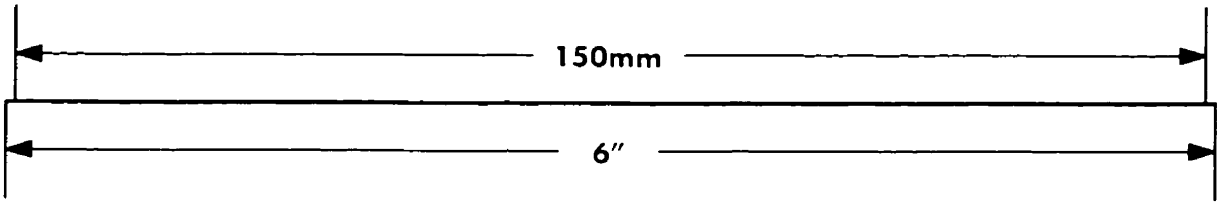

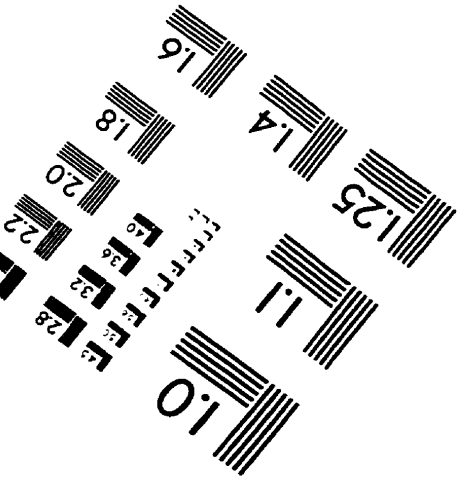

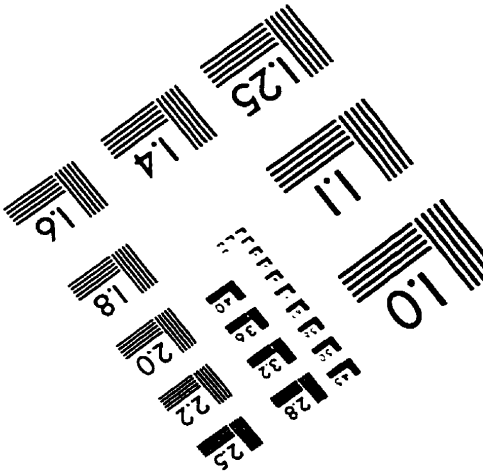

APPLIED IMAGE, Inc
1653 East Main Street
Rochester, NY 14609 USA
Phone: 716/482-0300
Fax: 716/288-5989